HHS Public Access

Author manuscript

Mol Cancer Res. Author manuscript; available in PMC 2024 February 01.

Published in final edited form as:

Mol Cancer Res. 2023 August 01; 21(8): 849–864. doi:10.1158/1541-7786.MCR-22-0898.

MDM2 inhibition enhances immune checkpoint inhibitor efficacy by increasing IL-15 and MHC class II production

Marlene Langenbach[1,2,*], **Sophie Giesler**[1,*], **Stefan Richtsfeld**[1,*], **Sara Costa-Pereira**[3], **Lukas Rindlisbacher**[3], **Tobias Wertheimer**[3], **Lukas M. Braun**[1], **Geoffroy Andrieux**[4], **Sandra Duquesne**[1], **Dietmar Pfeifer**[1], **Nadine M. Woessner**[5,6], **Hans D. Menssen**[7], **Sanaz Taromi**[1], **Justus Duyster**[1], **Melanie Börries**[4,6], **Tilman Brummer**[8,9], **Bruce R. Blazar**[10], **Susana Minguet**[5], **Patrick Turko**[11], **Mitchell P. Levesque**[11,**], **Burkhard Becher**[3,**], **Robert Zeiser**[1,5,6,**]

[1]Department of Medicine I - Medical Center - University of Freiburg, Faculty of Medicine, University of Freiburg, Germany

[2]Faculty of Biology, Albert-Ludwigs-University, Freiburg, Germany

[3]Institute of Experimental Immunology, University of Zurich, Zurich, Switzerland

[4]Institute of Medical Bioinformatics and Systems Medicine, Medical Center - University of Freiburg, Germany. German Cancer Research Center (DKFZ), Heidelberg, Germany

[5]Signalling Research Centres BIOSS and CIBSS – Centre for Integrative Biological Signalling Studies, University of Freiburg

[6]Spemann Graduate School of Biology and Medicine (SGBM), Albert-Ludwigs-University Freiburg, Freiburg, Germany

[7]Novartis Pharma, Basel, Switzerland

Corresponding author: Robert Zeiser, MD, Department of Hematology, Oncology and Stem cell transplantation, University Medical Center Freiburg, Freiburg, D-79106 Freiburg, Germany, Tel: +49-761-270-34580, Fax: +49-761-270-73570, robert.zeiser@uniklinik-freiburg.de.

*Co-first authors

**Co-senior authors

Author contributions:

M.L., S.G. and S.R. performed the majority of the experiments, helped to develop the overall concept, analyzed data and helped to write the manuscript. S.C.P., L.R. and T.W. performed high resolution flow-cytometry and analysed data, L.M.B. helped with experiments, G.A. analysed gene expression data for the mouse samples, D.P. helped with microarrays, J.D. analysed data and helped with the manuscript, M.B. analysed microarray data, T.B. provided vital reagents and discussed data, N.M.W. and S.M. helped with Ca^{2+} flux experiments and data analysis, H.D.M. provided vital reagents, helped with data analysis and the manuscript, B.R.B. helped with vital reagents and helped with data analysis and writing of the manuscript, P.T. and M.P.L. provided de-identified patient derived melanoma cells, analysed human gene expression data, and helped with the manuscript, B.B. supervised high resolution flow cytometry based analysis of the tumor tissue, R.Z. developed the overall concept, supervised the experiments, analyzed data and wrote the manuscript.

Data sharing:

The authors declare that the database is open to the scientific and medical community upon request to the senior author. Microarray data are deposited in the database GEO repository under the GEO accession number GSE184524.

Conflict-of-interest:

B.R.B. receives remuneration as an advisor to Magenta Therapeutics and BlueRock Therapeutics; Research funding from BlueRock Therapeutics, Rheos Medicines, Equilibre biopharmaceuticals, Carisma Therapeutics, Inc., and is a co-founder of Tmunity Therapeutics. R.Z. received honoraria from Novartis, Incyte, Sanofi, VectivBio and MNK outside of the submitted work. H.D.M. holds a patent application for the use of MDM2-inhibition to prevent or treat leukemia relapse post allo-HCT (PCT/EP2021/075896). H.D.M. is an employee of Novartis. The other authors have no conflict of interest in direct relation to this work to disclose.

[8]German Cancer Consortium (DKTK), partner site Freiburg, and German Cancer Research Center (DKFZ) Heidelberg, Germany

[9]Institute of Molecular Medicine and Cell Research (IMMZ), Faculty of Medicine, University of Freiburg, Freiburg, Germany Germany

[10]Masonic Cancer Center and Department of Pediatrics, Division of Blood and Marrow Transplant & Cellular Therapy, University of Minnesota, Minneapolis, Minnesota, USA

[11]Department of Dermatology, University Hospital Zurich, Zurich, Switzerland

Abstract

The treatment of metastatic melanoma patients with immune checkpoint inhibitors (ICI) leads to impressive response rates but primary and secondary resistance to ICI reduce progression-free survival. Novel strategies that interfere with resistance mechanisms are key to further improve patient outcome during ICI therapy. P53 is often inactivated by mouse-double-minute-2 (MDM2), which may decrease immunogenicity of melanoma cells.

We analyzed primary patient-derived melanoma cell lines, performed bulk sequencing analysis of patient-derived melanoma samples and used melanoma mouse models to investigate the role of MDM2-inhibition for enhanced ICI therapy.

We found increased expression of IL-15 and MHC-II in murine melanoma cells upon p53 induction by MDM2-inhibition. MDM2-inhibitor induced MHC-II and IL-15-production, which was p53 dependent as p53 knockdown blocked the effect. Lack of IL-15-receptor in hematopoietic cells or IL-15 neutralization reduced the MDM2-inhibition/p53-induction mediated anti-tumor immunity. p53 induction by MDM2-inhibition caused anti-melanoma immune memory as T cells isolated from MDM2-inhibitor treated melanoma bearing mice exhibited anti-melanoma activity in secondary melanoma-bearing mice. In patient-derived melanoma cells p53 induction by MDM2-inhibition increased IL-15 and MHC-II. IL-15 and CIITA expression was associated with a more favorable prognosis in patients bearing WT but not *TP53* mutated melanoma.

Implications: MDM2-inhibition represents a novel strategy to enhance IL-15 and MHC-II-production, which disrupts the immunosuppressive tumor microenvironment. Based on our findings a clinical trial combining MDM2-inhibition with anti-PD-1 immunotherapy for metastatic melanoma is planned.

Keywords

immune checkpoint inhibitor; mouse-double-minute-2-inhibition; melanoma; IL-15; MHC-II; tumor microenvironment

Introduction

The treatment of metastatic melanoma patients with immune checkpoint inhibitors (ICI) leads to impressive response rates and improved overall survival (1). However, primary and secondary resistance to ICI reduce progression-free survival (2). Novel strategies that interfere with resistance mechanisms are key to further improve patient outcome

during ICI therapy. The host factors that cause ICI-resistance include patient-related factors such as physical performance status, microbiome, immune status, and medication. Tumor-related factors include the proliferative activity, driver mutations, mutational burden and a non-inflamed tumor microenvironment. The non-inflamed tumor microenvironment can be potentially overcome by inducing local inflammation and pro-inflammatory cytokine production. Oncogenes and oncogenic signaling may promote immune escape as shown for example for c-myc through CD47 and PD-L1 (3). Signaling upon reduced expression of the tumor suppressor p53 may also cause immune escape.

Interleukin-15 (IL-15) is an activator of cytotoxic T cells and natural killer (NK) cells. A recent clinical trial using IL-15 treatment in patients with metastatic malignancies revealed expansion of NK cells, γδ T cells and $CD8^+$ memory T cells as well as tumor regression in some patients (4). We have previously shown that FLT3-inhibition can lead to reduction of ATF4 which in turn increased IRF7 activation and consecutive IL-15 production by FLT3-ITD mutant leukemia cells, which enhanced anti-tumor immune responses in mice (5). The activity of FLT3-inhibition against FLT3-ITD mutant leukemia was also observed in a randomized placebo-controlled clinical trial (6). Melanoma cells may downregulate IL-15 production and MHC expression to escape immune responses. Our previous work has shown that microRNA-146a production by melanoma cells is a mechanism by which melanoma cells escape IFN-γ mediated immune responses (7). Mouse double minute-2 (MDM2) inhibitors (8, 9) can induce p53-dependent apoptosis in different cancer cell types, however their role in shaping anti-cancer immune responses is unclear so far. The MDM2 protein is an ubiquitin ligase that recognizes the N-terminal trans-activation domain of p53 thereby inhibiting p53 transcriptional activation. Conversely, MDM2-inhibition increases p53 activity (9). Besides its effects on cell cycle, apoptosis and DNA-repair, p53 can also increase the expression of certain immune-related genes as shown in the setting of anti-viral immunity (10).

We observed that mouse-double-minute-2 (MDM2)-inhibition induced p53 which in turn caused the transcription of IL-15 and MHC class II in melanoma cells. Using loss-of-function approaches for IL-15 receptor or antibody-based IL-15 blockade we could prove a functional role for IL-15 in anti-cancer immunity induced by MDM2-inhibition.

In agreement with these studies in mice we observed in melanoma patients that IL-15 expression correlated with survival when p53 was wildtype.

Material and Methods:

Human samples and data analysis

Primary patient-derived melanoma cell lines were derived from a live-cell biobank containing heterogeneous melanoma cells from native biopsies (11) provided by the Department of Dermatology, University Hospital Zurich, Zurich, Switzerland. Bulk RNA-seq data from skin cutaneous melanoma, with associated clinical information, was obtained from The Cancer Genome Atlas (TCGA) using the R/bioconductor package curatedTCGAdata (12). RNA-seq data was converted to counts per million (CPM) and then normalized using the housekeeping genes ABCF1, DNAJC14, ERCC3, G6PD,

GUSB, MRPL19, NRDE2, OAZ1, POLR2A, PSMC4, PUM1, SDHA, SF3A1, STK11IP, TBC1D10B, TBP, TFRC, TLK2, TMUB2, and UBB. Housekeeping normalization was performed by dividing the expression of all genes by the geometric mean of the housekeeping gene expressions. Samples were limited to primary and metastatic tumors, and were merged by patient, leaving 101 and 368 samples, respectively. For each of the target genes MDM2, C2TA, and IL-15, the top and bottom quartiles were defined as “high” and “low” expressing samples.

qPCR primer sequences are listed in Suppl. Table S1, Flow cytometry antibodies are shown in Suppl. Table S2, Western blot antibodies are listed in Suppl. Table S3. TP53, BRAF and NRAS mutational status of each cell line was assessed by sequencing (Suppl. Table S4).

Survivorship—For each of the target genes, survivorship differences between the “high” and “low” groups were assessed using the Log-Rank test.

Correlation with IFN signature—The log10-transformed expression of each of the target genes was compared to the log10-transformed expression of the Type I Interferon (alpha/beta IFN) pathway in each sample. First, expression of the target gene was correlated with each individual gene in the IFN pathway. Second, target gene expression was correlated with an overall pathway score, which was computed by taking the mean expression of all genes in the pathway. For both of the above tests, we assessed Pearson’s correlation coefficient R and the *p*-value from a linear model. Third, we performed a *t*-test comparing the overall pathway scores of the “high” and “low” expressing groups. Finally, we performed unsupervised hierarchical clustering of samples based on their expression of genes in the IFN signature.

Cell type deconvolution and imputation of cell-type specific gene expression —We used CIBERSORTx (13) to infer the fractions of cell types present in each sample. First, deconvolution was performed separately to infer fractions of broad cell types and for a set of 22 immune cell types, using curated cell-type signatures provided by CIBERSORTx. Second, in high-resolution mode, the expression levels of each of our target genes was inferred per cell type.

Cell lines

B16.F10 murine melanoma cell line was provided by Prof. H. Pircher, Freiburg, Germany. Transducing the cells with a lentiviral vector containing firefly luciferase, a neomycin resistance gene, and green-fluorescent protein (GFP) produced a transgenic line of the B16.F10 luc^+ GFP^+. B16.F10 luc^+ were selected with 2 mg/ml of the neomycin analog geneticin (G-418 Sulfate). *TP53* knockdown B16.F10 *TP53* KD and the control B16.F10 *Renilla* were generated by retroviral transduction with a *TP53* shRNA-containing vector (see Suppl. Methods). B16.F10 parental, B16.F10 luc^+, B16.F10 *TP53*KD and B16.F10 *Renilla* were authenticated by Microsynth (Switzerland). $BRAF^{V600E}$-mutant 4434 mouse melanoma cell lines (14) were established from C57BL/6 LSL-$Braf^{V600E}$; *Tyr*::$CreERT^{2+/o}$ mice and were provided by Dr. Richard Marais, Manchester, UK. $BRAF^{V600E}$ mutational

status was confirmed by genotyping (see Suppl. Methods). All cells were cultured at 37 °C in 5 % CO_2.

Mice

C57BL/6 (H-2Kb) mice were purchased either from Janvier Labs (France) or obtained from the local stock of the animal facility at University Medical Center Freiburg, Germany. B6;129X1-*Il-15ra*$^{(tm1Ama)}$/J mice were provided by Prof. Dr. Burkhard Becher from the University of Zurich. Mice were used between 6 and 14 weeks of age, 15–25 mg of weight, and only female or male donor/recipient pairs were used. All animal studies were approved by the animal ethics committee Regierungspräsidium Freiburg, Freiburg, Germany (Protocol approval numbers: G17–049, X15–10A, X20–06K).

Mouse melanoma models

WT C57BL/6 mice were injected with 5000 or 10 000 B16.F10 luc$^+$ melanoma cells in the tail vein. Afterwards, their survival was monitored and bioluminescence images (BLI) were captured as described previously (15). In another experiment, the mice were sacrificed on day 12 or 13 and the organs were resected for further examination. For the second melanoma model, 2×10^6 4434 melanoma cells were injected intravenously (i.v.) in the tail vein and survival was monitored.

Subcutaneous models for melanoma involved injection of 1×10^6 B16.F10 luc$^+$ melanoma cells into WT C57BL/6 mice. Tumor growth was monitored via palpation and BLI. The tumors and organs were isolated from mice euthanized on day 13.

Flow cytometry

For high dimensional analysis of spectral flow cytometry data, cells were stained using the antibodies specified in Supplementary Table 2. The detailed methods are described in the Suppl. Methods part.

Statistical analysis

For the sample size in the murine experiments a power analysis was performed. A sample size of at least n=10 per group was determined by 80 % power to reach a statistical significance of 0.05 to detect an effect size of at least 1.06. Differences in animal survival (Kaplan-Meier survival curves) were analyzed by Mantel Cox test. The experiments were performed in a non-blinded fashion.

For statistical analysis of two groups an unpaired two-tailed Student's *t*-test was applied. All data were tested for normality applying the Kolmogorov-Smirnov test. If the data did not meet the criteria of normality, the Mann-Whitney *U* test was applied. If more than 2 groups were analyzed, we used the Kruskal-Wallis-Test if non-parametric testing was suggested and we performed a one-way ANOVA in case of normally distributed data. The *p*-values of fold changes were calculated using a one sample *t*-test or a one sample Wilcoxon Signed Rank test, if the data were not normally distributed. Statistical analysis was performed using GraphPad Prism (GraphPad Software; San Diego, CA). Data are presented as mean and s.e.m. (error bars). Differences were considered significant when the *p*-value was <0.05.

Data availability statement:

All data are available from the authors upon request. Microarray data are deposited in the database GEO repository under the GEO accession number GSE184524.

All other methods can be found in the Suppl. Methods part.

Results

MDM2-inhibition induces p53 and MHC class I and II expression in melanoma cells

Previous observations showed that the B16 melanoma microenvironment is immunosuppressive (7) and we hypothesized that MDM2-inhibition may be able to disrupt this state. To characterize the impact of MDM2-inhibition on the melanoma microenvironment, we analyzed the gene expression of subcutaneous B16 melanoma tissue isolated from mice treated with anti-PD-1 antibody and vehicle or anti-PD-1 antibody and MDM2-inhibitor. We observed that MDM2-inhibition induced the transcription of multiple genes related to IFN-γ signaling in subcutaneous B16 melanoma tissue (Fig. 1A). This was of specific interest since it was shown that tumors responding to ICI therapy exhibit a type-II IFN signature indicative of a T cell-inflamed phenotype (16). IFN-dependent genes such as MHC-II molecules were transcribed upon MDM2-inhibition (Fig. 1A). Additionally, multiple genes related to inflammatory signaling were upregulated upon MDM2-inhibition (Fig. 1B). These 2 pathways are within the 5 most differentially regulated pathways between tumors treated with anti-PD-1 alone or combined to MDM2 inhibitors. The 10 most differentially upregulated and downregulated pathways between tumors treated with anti-PD-1 alone or combined to MDM2 inhibitors are shown in Suppl. Figure 1A, B. To validate the gene expression data, we analyzed MHC-II protein expression in melanoma cells exposed to two different MDM2-inhibitors (HDM201, RG7112). We observed that MDM2-inhibition induced MHC-II (Fig. 1C–F) and MHC-I (Suppl. Fig. 2A–D) protein expression in murine B16 melanoma cells *in vitro* at concentrations that were non-toxic (Suppl. Fig. 2E, F).

To validate the role of MDM2 in human samples, we next analyzed melanoma cells derived from patients concerning the effects of MDM2 inhibition at concentrations that were non-toxic (Suppl. Fig. 2G). We observed that MDM2-inhibition caused upregulation of intracellular p53 and MDM2 as a positive feedback loop in response to the MDM2-inhibition in patient-derived melanoma cell lines (Fig. 1G, H) and in murine melanoma cells (Suppl. Fig. 2H). Since this finding indicates that p53 activation causes high MDM2 levels in patients, we analyzed whether high MDM2 levels correlated with gene expression signatures in patients. In agreement with the findings in mice, type I Interferon (alpha/beta IFN) pathway expression significantly correlated with the expression of MDM2 (Fig. 1I). Unsupervised clustering of samples based on IFN pathway gene expression successfully separated “high” and “low” MDM2 expressing samples (Fig. 1J). These findings indicate that in mice and patient-derived cell lines MDM2-inhibition leads to high MDM2 levels and the expression of a pro-inflammatory type I Interferon gene response.

MDM2-inhibition induced p53 improves anti-melanoma immune responses *in vivo* and increases the frequency of $CD8^+CD73^+TCF\text{-}1^+IFN\gamma^+TNF^+$ T cells

To assess the impact of p53 induction by MDM2-inhibition on anti-melanoma T cell responses in vivo, we analyzed the survival of mice in the absence of anti-PD-1-treatment. MDM2-inhibition alone did not improve survival of melanoma-bearing mice (Fig. 2A). Conversely, MDM2-inhibition led to improved survival of melanoma-bearing mice treated with anti-PD-1 antibodies (Fig. 2B). This survival pattern was reproducible in a second model with higher B16 melanoma burden (Suppl. Fig. 3). Improved survival correlated with a lower bioluminescence signal in MDM2-inhibitor treated compared to vehicle treated mice bearing luciferase- and GFP-expressing metastatic melanoma cells (Fig. 2C, D). Additionally, the frequencies of macroscopic lung metastases and GFP^+ melanoma cells in the lungs were lower in MDM2-inhibitor-treated compared to vehicle-treated melanoma-bearing mice (Fig. 2E, F).

To characterize the changes in the $CD8^+$ T cell compartment upon anti-PD-1 and MDM2-inhibition in the lungs of mice with metastatic melanoma, we performed high dimensional single cell analyses (Suppl. Fig. 4A, B). T cell factor-1 (TCF-1) was shown to drive the maintenance of the immune response of $CD8^+$ T cells after PD-1 checkpoint blockade therapy (17, 18). Resorting to unsupervised representation learning techniques and self-organizing maps meta-clustering based, we observed an increased frequency of $CD8^+CD73^+TCF\text{-}1^+IFN\gamma^+TNF^+$ T cells derived from the lungs of MDM2-inhibitor/anti-PD-1-treated compared to vehicle/anti-PD-1-treated melanoma-bearing mice (Fig. 2G, H). Additionally, $CD8^+$ T cells derived from the lungs of MDM2-inhibitor/anti-PD-1-treated mice expressed increased longevity T cell markers TCF-1 and CD127 (IL-7R) and the activation marker CD25 compared to vehicle/anti-PD-1-treated melanoma-bearing mice (Fig. 2I–K). Multiple other markers were not different between the groups, although there was a trend towards lower $CD8^+TOX^+$ T cells in the lungs of MDM2-inhibitor/anti-PD-1-treated compared to vehicle/anti-PD-1-treated melanoma-bearing mice (Suppl. Fig. 5A–C).

To test the effect of MDM2-inhibition in a second model, we used a subcutaneous melanoma model and observed that the bioluminescence signal derived from the tumor cells was lower in the anti-PD-1/MDM2-inhibitor treated melanoma bearing mice compared to the anti-PD-1/vehicle group (Fig. 2L). To understand if the improved melanoma control was associated with a higher T cell activation status, we analyzed T cells isolated from mice treated with anti-PD-1 with or without MDM2-inhibitor for calcium influx upon TCR stimulation. We found that T cells from the mice treated with the MDM2-inhibitor exhibited a higher calcium response upon TCR stimulation (Fig. 2M). To analyze if the efficacy of T cells in MDM2-inhibitor treated melanoma-bearing mice against melanoma cells is enhanced compared to T cells from vehicle-treated melanoma-bearing mice, we isolated T cells from such mice and transferred them into secondary recipient melanoma-bearing mice. Transfer of T cells isolated from MDM2-inhibitor treated mice improved survival of recipient melanoma-bearing mice compared to secondary recipient melanoma-bearing mice treated with T cells isolated from vehicle treated mice (Fig. 2N). These findings indicate that MDM2-inhibition enhances efficacy of anti-PD-1 immunotherapy against melanoma in two

independent models, increases the frequency of $CD8^+CD73^+TCF\text{-}1^+IFN\gamma^+TNF^+$ T cells and promotes TCR activation and immune memory against melanoma cells.

IL-15 is induced by p53 upon MDM2-inhibition and hematopoietic IL-15R$^{-/-}$ mice exhibit reduced protective effects

Based on the central role of IL-15 for anti-tumor immune responses (19) and because we had previously shown that inhibition of oncogenic signaling can release IL-15 transcription (5), we studied the impact of MDM2-inhibition on IL-15 production by melanoma cells. MDM2-inhibition with two different MDM2-inhibitors (HDM201, RG7112) induced IL-15 expression in melanoma cells at the RNA (Fig. 3A) and protein level (Fig. 3B–E). Since IL-15 is only active in the context of IL-15Rα-trans-presentation, we also studied IL-15Rα which was increased upon MDM2-inhibition (Fig. 3F). The protective *in vivo* effects of MDM2-inhibition on survival and melanoma growth were reduced when IL-15 was neutralized with an anti-IL-15/anti-15Rα antibody (Fig. 3G–I). To study the role of IL-15Rα in the immune compartment, we generated bone marrow chimeras that lacked IL-15Rα in hematopoietic cells and compared these to mice that had received WT bone marrow. Lack of IL-15Rα reduced the protective MDM2-inhibitor effect on survival (Fig. 3J). We observed no difference in survival of mice that lacked IL-15Rα compared to WT control in hematopoietic cells when treated with isotype antibody only (Suppl. Figure 6A).

Since the IFN pathway gene expression signature was identified in melanoma tissue of MDM2-inhibitor treated mice we performed unsupervised clustering of expression of IFN pathway genes in human melanoma samples. This analysis separated “high” and “low” IL-15 expression samples (Fig. 3K). Stratification of the patients according to “high” and “low” IL-15 expressing samples led to the identification of a higher survival rate of patients with a “high IL-15” signature (Fig. 3L). High resolution analysis of gene expression revealed that also in patients, the melanoma cells themselves produced IL-15, besides cancer associated fibroblasts (CAF), macrophages and B cells (Fig. 3M).

The findings indicate that the p53/MDM2-inhibitor effect is mediated to some extent by IL-15 induction in mice and that a “high IL-15” signature is connected to a higher survival rate of patients with melanoma.

TNF and TNF-signaling related genes increase upon p53 induction by MDM2-inhibition in the tumor microenvironment

Further transcriptional analysis of the melanoma tumor microenvironment (TME) of B16.F10 melanoma tissue grown subcutaneously in mice revealed increased expression of TNF and TNF-related genes in melanoma-bearing mice treated with anti-PD-1 and MDM2-inhibitor compared to mice treated with anti-PD-1 plus vehicle. (Fig. 4A). To determine the origin of TNF in the TME, we analyzed $CD4^+$ T cells and found increased intracellular TNF levels in melanoma-bearing mice treated with MDM2-inhibitor compared to vehicle-treated mice (Fig. 4B, C). $CD8^+$ T cells in melanoma-bearing mice treated with MDM2-inhibitor exhibited higher BCL-2 levels compared to vehicle-treated mice (Fig. 4D, E). Consistent with reduced immunosuppressive activity we observed lower fold changes of percentage of $CD4^+Foxp3^+$ regulatory T cells in melanoma-bearing mice

treated with MDM2-inhibitor compared to vehicle-treated mice (Fig. 4F, G). High resolution immune-phenotyping revealed that $CD8^+TOX^+$ exhausted T cells isolated from the tumor itself were reduced in melanoma-bearing mice treated with MDM2-inhibitor/anti-PD-1 compared to vehicle/anti-PD-1-treated mice (Fig. 4H–I), while other populations were not significantly different between the groups (Suppl. Fig. 7A, B). The observation that $CD8^+TOX^+$ exhausted T cells isolated from the tumor itself were reduced is compatible with the observed trend towards reduced $CD8^+TOX^+$ exhausted T cells isolated from the lungs of tumor bearing mice (Suppl. Fig. 5B). $CD11b^+$ cells were increased in the melanoma tissue of mice treated with MDM2-inhibtor compared to vehicle-treated mice, while this difference was not seen in the lung tissue of melanoma bearing mice (Suppl. Fig. 8A, B). We found that the $CD8^+CD73^+TCF^+IFN\gamma^+TNF^+$ cells express only marginal levels of PD-1 (Suppl. Fig. 8C, D). The total $CD8^+TCF^+$ population showed PD-1 expression which was reduced after treatment with MDM2-inhibitor (Suppl. Fig. 8E, F). These findings indicate that MDM2-inhibition increases the frequency of activated TNF^+CD4^+ T cells and $BCL2^+CD4^+$ T cells, while reducing frequencies of Treg and $CD8^+TOX^+$ exhausted T cells in subcutaneously grown melanoma.

MDM2-inhibition affects p53 pathway activity in the melanoma microenvironment

Since MDM2-inhibition was shown to increase p53 activity (9), we analyzed the transcription of genes related to the p53 pathway. We observed the differential regulation of multiple p53-related genes upon MDM2-inhibition (Fig. 5A). Additionally, Transporter associated with antigen processing 1 (TAP1), a transporter involved in antigen presentation via MHC-II was upregulated upon MDM2-inhibition as well as MDM2 itself (Fig. 5A). To decipher the functional role of p53 in the MDM2-inhibitor mediated effects, we next generated *TP53* knockdown (*TP53* KD) B16 melanoma cells (Fig. 5B, Suppl. Fig. 9). *TP53* knockdown reduced the MDM2-inhibitor induced increase of MHC-II and IL-15 (Fig. 5C, D). To test the functional role of p53 in melanoma cells *in vivo,* we next used *Renilla*-shRNA-vector control or *TP53* KD melanoma cells. Melanoma-related mortality was not different when *Renilla*-shRNA-vector control or *TP53* KD melanoma cells were used in vehicle/anti-PD-1-treated mice (Fig. 5E). Conversely, the protective effect of MDM2-inhibitor/anti-PD-1 treated mice was abolished in *TP53* KD melanoma-bearing mice compared to *Renilla*-shRNA-vector control melanoma-bearing mice (Fig. 5E). Consistent with the role of the p53/IL-15 axis in mice we found that the survival advantage of patients with a “high IL-15” signature was detectable in patients with WT melanoma but not in patients with *TP53* mutant melanoma (Fig. 5F).

These findings indicate that the MDM2-inhibitor mediated immune effects via IL-15 require intact p53.

P53 induction by MDM2-inhibition is also active in *BRAF*^{V600E} mutated melanoma

BRAF somatic mutations are found in 66% of malignant melanomas (20) and BRAF-inhibition is a major therapeutic approach for *BRAF*^{V600E} mutated melanoma. To understand whether the findings made in *BRAF*-WT melanoma cells can be extended to *BRAF*^{V600E} mutated melanoma, we used the 4434 melanoma cell line (14) derived from *Braf*$^{+/LSL\text{-}BRAFV600E}$; *Tyr*::$CreER^{T2+/o}$ mice. We observed that BRAF-inhibition did

not interfere with the MDM2-inhibition induced IL-15 and MHC-I expression (Fig. 6A–D) at concentrations that were non-toxic (Suppl. Fig. 10). The protective effect of combined anti-PD-1 and MDM2 was not lost when a BRAF-inhibition was added (Fig. 6E). The protective effect of combined anti-PD-1, MDM2- and BRAF-inhibition was lost when mice were treated with anti-IL-15/anti-15Rα (Fig. 6F). In agreement, the combination of anti-PD-1, MDM2- and BRAF-inhibition was not effective in mice that lacked IL-15Rα in hematopoietic cells (Fig. 6G). BRAF-inhibition alone was not sufficient to cause survival beyond day 60, indicating that long-term melanoma control was via the synergism between anti-PD-1 and MDM2-inhibition. These findings indicate that MDM2-inhibition also has activity in *BRAF*^{V600E} mutated melanoma.

TP53 mutated patient-derived melanoma cells are resistant to MDM2-inhibition induced expression of the CIITA / HLA axis

To validate whether the effects of MDM2-inhibition on mouse melanoma cells could be reproduced in human primary melanoma cells, we next exposed melanoma cells derived from primary human melanoma biopsies to p53 induction by MDM2-inhibition. We observed increased HLA-DR (Fig. 7A) and HLA-A/B/C (Suppl. Fig. 11) expression upon MDM2-inhibition in melanoma cells derived from 8 different patients. The presence of *BRAF*^{V600E} and *NRAS* mutations, two important driver mutations in melanoma, had no impact on HLA-DR and HLA-A/B/C expression. CIITA is the transcriptional activator of HLA-DR. We performed unsupervised clustering of gene expression in human melanoma samples based on IFN pathway gene expression and observed that the gene expression signature separated “high” and “low” CIITA expressing samples (Fig. 7B). Stratification of the patients according to “high” and “low” CIITA expressing samples revealed a higher survival rate of patients with a “high CIITA” signature (Fig. 7C). The connection between the IFN pathway gene expression and “high” CIITA expression was reproducible in the presence of a *BRAF*^{V600E} mutation and *NRAS* mutations (Fig. 7D, E). We found increased IL-15 protein expression upon MDM2-inhibition in melanoma cells derived from 8 different patients (Fig. 7F). The presence of *BRAF*^{V600E} and NRAS mutations had no impact on IL-15 expression. A connection between the IFN pathway gene expression and “high” IL-15 expression was found in the presence of a *BRAF*^{V600E} mutation and *NRAS* mutations (Fig. 7G).

To understand if the observed effects were p53-dependent, we also studied *TP53* mutated patient-derived melanoma cells (TP53 Exon5 ENST00000269305: 76 (451) [chr17:g.7578479 (hg19)] c.451C>G, p.Pro151Ala VAF 100% (8405 reads) rs28934874 (ClinVar; dbSNP), COSM44944 (COSMIC)) (21). In the presence of the *TP53* mutation, MDM2-inhibition did not cause increases of MDM2 expression (Fig. 7H) nor of HLA-DR, HLA-A/B/C and IL-15 expression (Fig. 7I). These findings indicate that MDM2-inhibition induces expression of the CIITA / HLA axis and IL-15 in human primary melanoma cells in a p53-dependent manner and that CIITA-high expression correlates with improved survival in patients. Our findings are summarized in a graphical abstract (Suppl. Fig. 12).

Discussion

Overcoming resistance to anti-PD-1 immunotherapy in tumors with a low immune cell infiltration is a major task in order to improve progression-free survival of cancer patients (2). Here we identify p53 induction by MDM2-inhibition as a potent therapeutic strategy to enhance activity of anti-PD-1 immunotherapy against melanoma.

Our findings extend previous work showing that pharmacological activation of p53 triggers the expression of endogenous retroviruses (ERV), which was LSD1- and DNMT1-dependent (22). The authors found increased infiltration of cytotoxic $CD8^+$ T cells and tumor-suppressive M1 macrophages *in vivo* in a colon carcinoma model Colon26 upon treatment with stapled peptide MDM2 inhibitor ALRN-6924 (22). We extend this by showing that MDM2-inhibition induced p53 induction caused IL-15 and MHC-II expression, which is dependent on intact p53. Using IL-15R loss-of-function approaches and antibody-based IL-15 blockade we provide a functional role for IL-15 for the synergistic effect of MDM2-inhibition and anti-PD-1 immunotherapy. Consistent with our findings on the central role of IL-15 for melanoma regression, others had shown that the intratumoral delivery of an IL-15-expressing plasmid into established B16 murine melanoma tumors led to dramatic tumor regression (23). A similar observation was made when treating melanoma-bearing mice with an IL-15-IL-15Rα fusion protein (24). Additionally, it was shown that IL-15 treatment can convert “cold” tumors into “hot” tumors, by promoting lymphocyte infiltration into the TME (19).

Our finding on the p53/IL-15 axis induced by MDM2-inihibition extends other findings showing that MDM2 sustains STAT5 stability in T-cells which enhanced T-cell-mediated antitumor immunity in solid tumors (25). Since MDM2-inhibition with RG7112 causes upregulation of intracellular MDM2 as a positive feedback loop in response to the inhibition (26, 27), the increase of MDM2 in T-cells can directly enhance their anti-tumor activity (25). This is consistent with our observation that MDM2-inhibition increased MDM2 levels in human melanoma cells. Further, we show that MDM2 levels positively correlate with IFN-related gene signature in patient-derived melanoma. This indicates the association of p53 with an immunostimulatory microenvironment when using MDM2 expression level as a surrogate marker for high p53 transcriptional activity.

Besides the functional studies in the mouse model, we were able to validate our findings using patient-derived melanoma cells. Here we could link the MDM2-inihibitor induced IFN-related gene signature to increased expression of IL-15 and CIITA. Expression of IL-15 and CIITA correlated with the survival rate of patients indicating that these molecules contribute significantly to immunogenicity of the melanoma cells in patients. This effect was not seen when the melanoma cells had a *TP53* loss-of-function mutation. Consistent with an effect of MDM2-inhibition on T cells, we observed an increased frequency of $CD8^+CD73^+TCF\text{-}1^+IFN\gamma^+TNF^+$ T cells derived from the lungs of MDM2-inhibitor/anti-PD-1-treated compared to vehicle/anti-PD-1-treated melanoma-bearing mice. This could be connected to IL-15 production as the common gamma chain cytokine IL-15 promotes T cells survival and TCF-1 was shown to drive the maintenance of the immune response of $CD8^+$ T cells after PD-1 checkpoint blockade therapy (17, 18). Recent findings indicate

that treatment with tumor infiltrating lymphocytes (TIL) led to improved progression-free survival compared to ipilimumab in patients with advanced melanoma (28). Since MDM2-inhibition had a profound effect on IL-15 as shown by us and a direct effect on the T cells as shown by others (25) and us (27), a combination of TIL with MDM2-inhibition is a promising novel therapeutic concept.

The analysis of biopsy specimens from patients treated with the MDM2-inhibitor HDM201 revealed PD-1 and PD-L1 upregulation and an increase in $CD8^+$ tumor-infiltrating lymphocytes (29), which is consistent with our findings. In contrast to our work, this study did not assess the functional role of IL-15, MHC-I or MHC-II. Others have shown that MHC-II-expressing melanomas are eliminated by tumor-specific cytotoxic $CD4^+$ T-cells leading to tumor regression in an adoptive T cell transfer model (30, 31) and MHC-II expression in human melanoma cells is associated with response to anti-PD-1 treatment (32, 33). Conversely, another study reported an immunosuppressive effect of MHC-II expression on melanoma cells (34). Based on our finding that MDM2-inhibitors induce MHC-II expression on melanoma cells, we identify MHC-II upregulation by MDM2-inhibitors as a novel mechanism to increase sensitivity of malignant melanoma towards anti-PD-1 treatment. In mouse tumor models, the MDM2-inhibitor HDM201 induced an increase in the number of dendritic cells, in the percentage of T cells in tumors and tumor-draining lymph nodes, and in the ratio of $CD8^+$ T cells to regulatory T cells in tumors (29). Consistently we also observed reduced Treg frequencies in mice treated with the MDM2-inhibitor. However we extend these findings by high resolution flow-cytometry based analysis showing that p53 induction by MDM2-inhibition leads to increased frequency of $CD8^+CD73^+TCF\text{-}1^+IFN\gamma^+TNF^+$ T cells.

In summary, our findings in mouse models, patient-derived melanoma cells and transcriptional analyses of human melanoma samples indicate that p53-induction by MDM2-inhibition represents a novel strategy to enhance IL-15 and MHC-II-production in melanoma cells, which disrupts the immunosuppressive tumor microenvironment.

Supplementary Material

Refer to Web version on PubMed Central for supplementary material.

Acknowledgements:

Funding:

This study was supported by the Deutsche Forschungsgemeinschaft, Germany, SFB-1479 – Project ID: 441891347 (P01 to RZ, P14 to TB), SFB1160 TP B09 to R.Z., Project-ID 259373024 – TRR 167, DFG individual grant 872/4-2 to R.Z., the Deutsche Krebshilfe (grant number 70113473) and the Jose-Carreras Leukemia foundation grant number DJCLS 01R/2019 (R.Z.), the European Union: ERC-2022-ADG Project 101094168- AlloCure (ERC Advanced grant to R.Z.), Leukemia and Lymphoma society (award number 7030–23 to R.Z.) by the Germany's Excellence Strategy (CIBSS - EXC-2189 - Project ID 390939984 to R.Z.), MB is supported by the German Federal Ministry of Education and Research (BMBF) within the framework of the e:Med research and funding concept (coNfirm, FKZ 01ZX1708F) and within the Medical Informatics Funding Scheme (MIRACUM, FKZ 01ZZ1606A-H). This project has further received funding from the European Research Council (ERC) under the European Union's Horizon 2020 research and innovation programme grant agreement No 882424, the Swiss National Science Foundation (733 310030_170320, 310030_188450, and CRSII5_183478 to B.B.), the research initiative SKINTEGRITY (B.B.), Mertelsmann Foundation gGmbH, and the German research foundation fellowship to (TW). B.R.B. was supported by R01 HL155114, HL11879. The human data shown here are in part based upon

data generated by the TCGA Research Network: https://www.cancer.gov/tcga. The project was supported by the Lighthouse Core Facility (Medical Faculty, University of Freiburg - 2021/A2-Fol and - 2021/B3-Fol; DFG - 450392965).

References:

1. Larkin J, Chiarion-Sileni V, Gonzalez R, Grob JJ, Cowey CL, Lao CD, Schadendorf D, Dummer R, Smylie M, Rutkowski P, Ferrucci PF, Hill A, Wagstaff J, Carlino MS, Haanen JB, Maio M, Marquez-Rodas I, McArthur GA, Ascierto PA, Long GV, Callahan MK, Postow MA, Grossmann K, Sznol M, Dreno B, Bastholt L, Yang A, Rollin LM, Horak C, Hodi FS, Wolchok JD. Combined Nivolumab and Ipilimumab or Monotherapy in Untreated Melanoma. N Eng J Med. 2015;373:23–34.
2. van Elsas MJ, van Hall T, van der Burg SH. Future Challenges in Cancer Resistance to Immunotherapy. Cancers (Basel). 2020;12:935. [PubMed: 32290124]
3. Casey SC, Tong L, Li Y, Do R, Walz S, Fitzgerald KN, Gouw AM, Baylot V, Gütgemann I, Eilers M, Felsher DW. MYC regulates the antitumor immune response through CD47 and PD-L1. Science. 2016;352:227–31. [PubMed: 26966191]
4. Conlon KC, Lugli E, Welles HC, Rosenberg SA, Fojo AT, Morris JC, Fleisher TA, Dubois SP, Perera LP, Stewart DM, Goldman CK, Bryant BR, Decker JM, Chen J, Worthy TA, Figg WD Sr, Peer CJ, Sneller MC, Lane HC, Yovandich JL, Creekmore SP, Roederer M, Waldmann TA. Redistribution, hyperproliferation, activation of natural killer cells and CD8 T cells, and cytokine production during first-in-human clinical trial of recombinant human interleukin-15 in patients with cancer. J Clin Oncol. 2015;33:74–82. [PubMed: 25403209]
5. Mathew NR, Baumgartner F, Braun L, David Ó Sullivan, Thomas S, Waterhouse M, Müller TA, Hanke K, Taromi S, Apostolova P, Illert AL, Melchinger W, Duquesne S, Schmitt-Graeff A, Osswald L, Yan K-L., Weber A, Tugues S, Spath S, Pfeifer D, Follo M, Claus R, Lübbert M, Rummelt C, Bertz H, Wäsch R, Haag J, Schmidts A, Schultheiss M, Bettinger M, Thimme R, Ullrich E, Tanriver Y, Vuong GL, Arnold R, Hemmati P, Wolf D, Ditschkowski M, Jilg C, Wilhelm K, Leiber C, Gerull S, Halter J, Lengerke C, Pabst T, Schroeder T, Kobbe G, Rösler W, Doostkam S, Meckel S, Stabla K, Metzelder SK, Halbach S, Brummer T, Hu Z, Dengjel J, Hackanson B, Schmid C, Holtick U, Scheid C, Spyridonidis A, Stölzel F, Ordemann F, Müller LP, Sicre-de-Fontbrune F, Ihorst G, Kuball J, Ehlert JE, Feger D, Wagner EV, Cahn JY, Schnell J, Kuchenbauer F, Bunjes D, Chakraverty R, Richardson S, Gill S, Kröger N, Ayuk F, Vago L, Ciceri F, Müller AM, Kondo T, Teshima T, Klaeger S, Kuster B, Kim D, Weisdorf D, van der Velden W, Dörfel D, Bethge W, Hilgendorf I, Hochhaus A, Andrieux G, Börries M, Busch H, Magenau J, Reddy P, Labopin M, Antin J H, Henden AS, Hill GR, Kennedy GA, Bar M, Sarma A, McLornan D, Mufti G, Oran B, Rezvani K, Sha O, Negrin RS, Nagler A, Prinz M, Burchert A, Neubauer A, Beelen D, Mackensen A, von Bubnoff N, Herr W, Becher B, Socié G, Caligiuri MA, Ruggiero E, Bonini C, Häcker G, Duyster J, Finke J, Pearce E, Blazar BR, Zeiser R. Sorafenib promotes graft-versus-leukemia activity in mice and humans through IL-15 production in FLT3-ITD mutant leukemia cells. Nature medicine. 2018;24:282–91.
6. Burchert A, Bug G, Fritz LV, Finke J, Stelljes M, Röllig C, Wollmer E, Wäsch R, Bornhäuser M, Berg T, Lang F, Ehninger G, Serve H, Zeiser R, Wagner EM, Kröger N, Wolschke C, Schleuning M, Götze KS, Schmid C, Crysandt M, Eßeling E, Wolf D, Wang Y, Böhm A, Thiede C, Haferlach T, Michel C, Bethge W, Wündisch T, Brandts C, Harnisch S, Wittenberg M, Hoeffkes HG, Rospleszcz S, Burchardt A, Neubauer A, Brugger M, Strauch K, Schade-Brittinger C, Metzelder SK. Sorafenib Maintenance After Allogeneic Hematopoietic Stem Cell Transplantation for Acute Myeloid Leukemia With FLT3-Internal Tandem Duplication Mutation (SORMAIN). J Clin Oncol. 2020;10.
7. Mastroianni J, Stickel N, Andrlova H, Hanke K, Melchinger W, Duquesne S, Schmidt D, Falk M, Andrieux G, Pfeifer D, Dierbach H, Schmitt-Graeff A, Meiss F, Boerries M, Zeiser R. miR-146a Controls Immune Response in the Melanoma Microenvironment. Cancer Res. 2019;79:183–95. [PubMed: 30425059]
8. Kojima K, Konopleva M, Samudio IJ, et al. MDM2 antagonists induce p53-dependent apoptosis in AML: implications for leukemia therapy. Blood. 2008;106:3150–9.

9. Vassilev LT, Vu BT, Graves B, Carvajal D, Podlaski F, Filipovic Z, Kong N, Kammlott U, Lukacs C, Klein C, Fotouhi N, Liu EA. In vivo activation of the p53 pathway by small-molecule antagonists of MDM2. Science. 2004;303:844–8. [PubMed: 14704432]
10. Muñoz-Fontela C, Macip S, Martínez-Sobrido L, Brown L, Ashour J, García-Sastre A, Lee SW, Aaronson SA Transcriptional role of p53 in interferon-mediated antiviral immunity. J Exp Med. 2008;205:1929–38. [PubMed: 18663127]
11. Raaijmakers MI, Widmer DS, Maudrich M, Koch T, Langer A, Flace A, Schnyder C, Dummer R, Levesque MP. A new live-cell biobank workflow efficiently recovers heterogeneous melanoma cells from native biopsies. Exp Dermatol. 2015;24:377–80. [PubMed: 25739758]
12. Ramos M, Geistlinger L, Oh S, Schiffer L, Azhar R, Kodali H, de Bruijn I, Gao J, Carey VJ, Morgan M, Waldron L. Multiomic Integration of Public Oncology Databases in Bioconductor. JCO Clin Cancer Inform. 2020;4:958–71. [PubMed: 33119407]
13. Newman AM, Steen CB, Liu CL, Gentles AJ, Chaudhuri AA, Scherer F, Khodadoust MS, Esfahani MS, Luca BA, Steiner D, Diehn M, Alizadeh AA. Determining cell type abundance and expression from bulk tissues with digital cytometry. Nat Biotechnol. 2019;37:773–82. [PubMed: 31061481]
14. Hirata E, Girotti MR, Viros A, Hooper S, Spencer-Dene B, Matsuda M, Larkin J, Marais R, Sahai E. Intravital imaging reveals how BRAF inhibition generates drug-tolerant microenvironments with high integrin β1/FAK signaling. Cancer Cell. 2015;27:574–88. [PubMed: 25873177]
15. Andrlová H, Mastroianni J, Madl J, Kern JS, Melchinger W, Dierbach H, Follo M, Technau-Hafsi K, Has C, Mittapalli VR, Idzko M, Herr R, Brummer T, Ungefroren H, Busch H, Boerries M, Narr A, Ihorst G, Vennin C, Schmitt-Graeff A, Minguet S, Timpson P, Duyster J, Meiss F, Römer W, Zeiser R. Biglycan expression in the melanoma microenvironment promotes invasiveness via increased tissue stiffness inducing integrin-β1 expression. Oncotarget. 2017;8:42901–16. [PubMed: 28476030]
16. Gajewski TF, Corrales L, Williams J, Horton B, Sivan A, Spranger S. Cancer immunotherapy targets based on understanding the T cell-inflamed versus non-T cell-inflamed tumor microenvironment. Adv Exp Med Biol. 2017;1036:19–31. [PubMed: 29275462]
17. Chen Z, Ji Z, Ngiow SF, Manne S, Cai Z, Huang AC, Johnson J, Staupe RP, Bengsch B, Xu C, Yu S, Kurachi M, Herati RS, Vella LA, Baxter AE, Wu JE, Khan O, Beltra JC, Giles JR, Stelekati E, McLane LM, Lau CW, Yang X, Berger SL, Vahedi G, Ji H, Wherry EJ. TCF-1-Centered Transcriptional Network Drives an Effector versus Exhausted CD8 T Cell-Fate Decision. Immunity. 2019;51:840–55. [PubMed: 31606264]
18. Siddiqui I, Schaeuble K, Chennupati V, Fuertes Marraco SA, Calderon-Copete S, Pais Ferreira D, Carmona SJ, Scarpellino L, Gfeller D, Pradervand S, Luther SA, Speiser DE, Held W. Intratumoral Tcf1(+)PD-1(+)CD8(+) T Cells with Stem-like Properties Promote Tumor Control in Response to Vaccination and Checkpoint Blockade Immunotherapy. Immunity. 2019;50:195–211.e10. [PubMed: 30635237]
19. Bergamaschi C, Stravokefalou V, Stellas, Karaliota S, Felber BK, Pavlakis GN. Heterodimeric IL-15 in Cancer Immunotherapy. Cancers (Basel). 2021;13:837. [PubMed: 33671252]
20. Davies H, Bignell GR, Cox C, Stephens P, Edkins S, Clegg S, Teague J, Woffendin H, Garnett MJ, Bottomley W, Davis N, Dicks E, Ewing R, Floyd Y, Gray K, Hall S, Hawes R, Hughes J, Kosmidou V, Menzies A, Mould C, Parker A, Stevens C, Watt S, Hooper S, Wilson R, Jayatilake H, Gusterson BA, Cooper C, Shipley J, Hargrave D, Pritchard-Jones K, Maitland N, Chenevix-Trench G, Riggins GJ, Bigner DD, Palmieri G, Cossu A, Flanagan A, Nicholson A, Ho JW, Leung SY, Yuen ST, Weber BL, Seigler HF, Darrow TL, Paterson H, Marais R, Marshall CJ, Wooster R, Stratton MR, Futreal PA. . Mutations of the BRAF gene in human cancer. Nature. 2002;417:949–54. [PubMed: 12068308]
21. Chang MT, Asthana S, Gao SP, Lee BH, Chapman JS, Kandoth C, Gao J, Socci ND, Solit DB, Olshen AB, Schultz N, Taylor BS. Identifying recurrent mutations in cancer reveals widespread lineage diversity and mutational specificity. Nat Biotechnol. 2016;34:155–63. [PubMed: 26619011]
22. Zhou X, Singh M, Sanz Santos G, Guerlavais V, Carvajal LA, Aivado M, Zhan Y, Oliveira MMS, Westerberg LS, Annis DA, Johnsen JI, Selivanova G. Pharmacological activation of p53 triggers

viral mimicry response thereby abolishing tumor immune evasion and promoting anti-tumor immunity. Cancer Discov. 2021;11:3090–105. [PubMed: 34230007]

23. Ugen KE, Kutzler MA, Marrero B, Westover J, Coppola D, Weiner DB, Heller R. Regression of subcutaneous B16 melanoma tumors after intratumoral delivery of an IL-15-expressing plasmid followed by in vivo electroporation. Cancer Gene Ther. 2006;10:969–74.
24. Bessard A, Solé V, Bouchaud G, Quéméner A, Jacques Y. High antitumor activity of RLI, an interleukin-15 (IL-15)-IL-15 receptor alpha fusion protein, in metastatic melanoma and colorectal cancer. Mol Cancer Ther. 2009;9:2736–45.
25. Zhou J, Kryczek I, Li S, Li X, Aguilar A, Wei S, Grove S, Vatan L, Yu J, Yan Y, Liao P, Lin H, Li J, Li G, Du W, Wang W, Lang X, Wang W, Wang S, Zou W. The ubiquitin ligase MDM2 sustains STAT5 stability to control T cell-mediated antitumor immunity. Nat Immunol. 2021;22:460–70. [PubMed: 33767425]
26. Tovar C, Graves B, Packman K, Filipovic Z, Higgins B, Xia M, Tardell C, Garrido R, Lee E, Kolinsky K, To KH, Linn M, Podlaski F, Wovkulich P, Vu B, Vassilev LT. . MDM2 small-molecule antagonist RG7112 activates p53 signaling and regresses human tumors in preclinical cancer models. Cancer Res. 2013;73:2587–97. [PubMed: 23400593]
27. Ho JNHG, Schmidt D, Lowinus T, Ryoo J, Dopfer EP, Gonzalo Núñez N, Costa-Pereira S, Toffalori C, Punta M, Fetsch V, Wertheimer T, Rittmann MC, Braun LM, Follo M, Briere C, Vinnakota JM, Langenbach M, Koppers F, Shoumariyeh K, Engel H, Rückert T, Märklin M, Holzmayer S, Illert AL, Magon F, Andrieux G, Duquesne S, Pfeifer D, Staniek J, Rizzi M, Miething C, Köhler N, Duyster J, Menssen HD, Boerries M, Buescher JM, Cabezas-Wallscheid N, Blazar BR, Apostolova P, Vago L, Pearce EL, Becher B, Zeiser R. Targeting MDM2 enhances anti-leukemia immunity after allogeneic transplantation via MHC-II and TRAIL-R1/2 upregulation. Blood. 2022;140:1167–81. [PubMed: 35853161]
28. Haanen JBAG, Rohaan M, Borch TH et al. Treatment with tumor infiltrating lymphocytes (TIL) versus ipilimumab (IPI) for advanced melanoma: results from a multicenter, randomized phase 3 trial. Annals of Oncology. 2022;33:Supplement 7.
29. Wang HQ, Mulford IJ, Sharp F, Liang J, Kurtulus S, Trabucco G, Quinn DS, Longmire TA, Patel N, Patil R, Shirley MD, Chen Y, Wang H, Ruddy DA, Fabre C, Williams JA, Hammerman PS, Mataraza J, Platzer B, Halilovic E. Inhibition of MDM2 Promotes Antitumor Responses in p53 Wild-Type Cancer Cells through Their Interaction with the Immune and Stromal Microenvironment. Cancer Res. 2021;81:3079–91. [PubMed: 33504557]
30. Quezada SA, Simpson TR, Peggs KS, Merghoub T, Vider J, Fan X, Blasberg R, Yagita H, Muranski P, Antony PA, Restifo NP, Allison JP. Tumor-reactive CD4(+) T cells develop cytotoxic activity and eradicate large established melanoma after transfer into lymphopenic hosts. J Exp Med. 2010;207:637–50. [PubMed: 20156971]
31. Xie Y, Akpinarli A, Maris C, Hipkiss EL, Lane M, Kwon EK, Muranski P, Restifo NP, Antony PA. Naive tumor-specific CD4(+) T cells differentiated in vivo eradicate established melanoma. J Exp Med. 2010;207:651–67. [PubMed: 20156973]
32. Johnson DB, Estrada MV, Salgado R, Sanchez V, Doxie DB, Opalenik SR, Vilgelm AE, Feld E, Johnson AS, Greenplate AR, Sanders ME, Lovly CM, Frederick DT, Kelley MC, Richmond A, Irish JM, Shyr Y, Sullivan RJ, Puzanov I, Sosman JA, Balko JM. Melanoma-specific MHC-II expression represents a tumour-autonomous phenotype and predicts response to anti-PD-1/PD-L1 therapy. Nat Commun. 2016;7:10582. [PubMed: 26822383]
33. Rodig SJ, Gusenleitner D, Jackson DG, Gjini E, Giobbie-Hurder A, Jin C, Chang H, Lovitch SB, Horak C, Weber JS, Weirather JL, Wolchok JD, Postow MA, Pavlick AC, Chesney J, Hodi FS. MHC proteins confer differential sensitivity to CTLA-4 and PD-1 blockade in untreated metastatic melanoma. Science translational medicine. 2018;450:eaar3342.
34. Nirmal AJ, Maliga Z, Vallius T, Quattrochi B, Chen AA, Jacobson CA, Pelletier RJ, Yapp C, Arias-Camison R, Chen YA, Lian CG, Murphy GF, Santagata S, Sorger PK. The Spatial Landscape of Progression and Immunoediting in Primary Melanoma at Single-Cell Resolution. Cancer Discov. 2022;12:1518–41. [PubMed: 35404441]

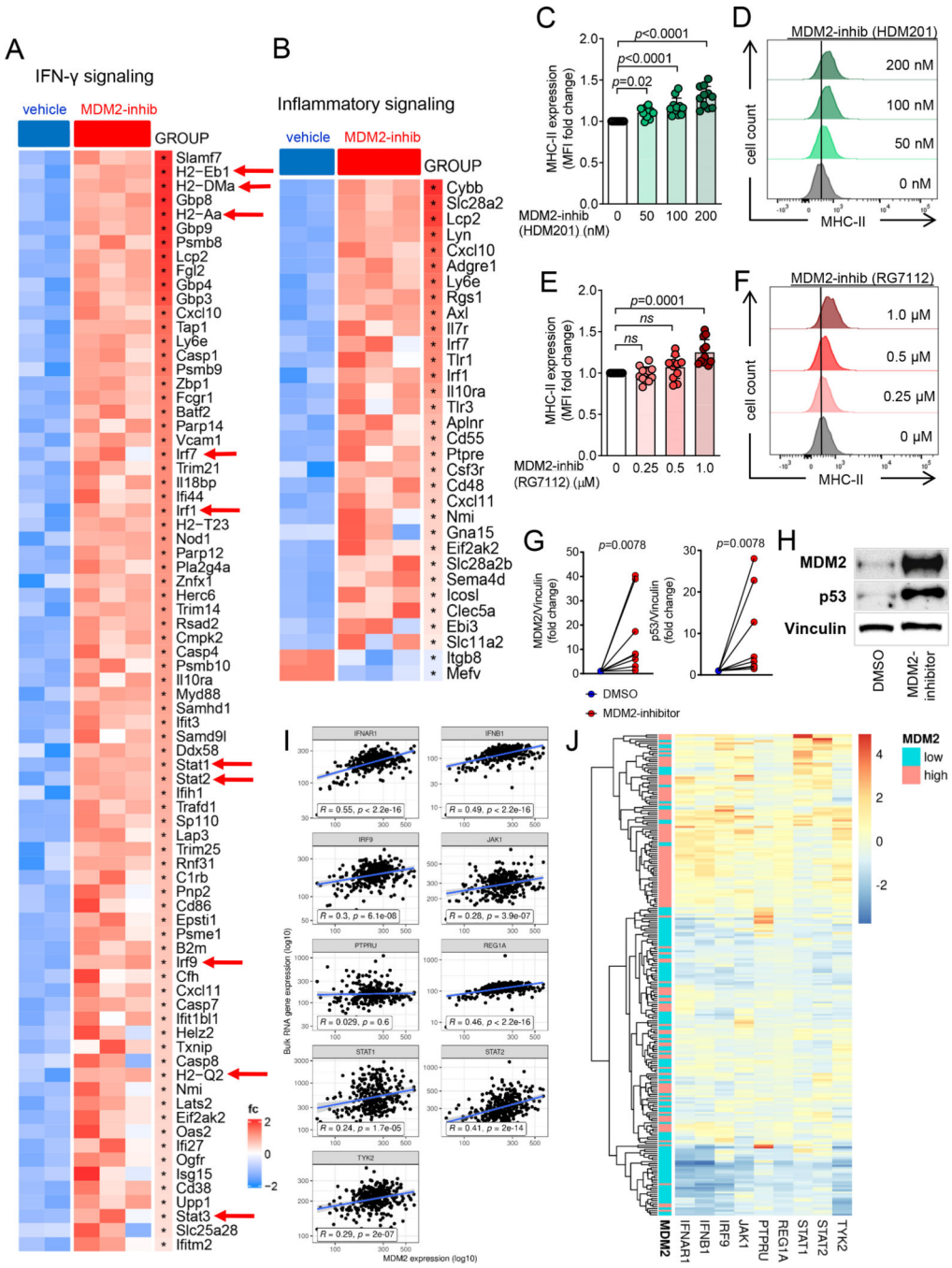

Fig. 1: MDM2-inhibition induces expression of genes related to IFN-γ signaling in the melanoma microenvironment in mice and patients.

(A, B) Relative expression, as microarray heatmap ("Z-score intensity"), of RNA isolated from subcutaneous B16.F10 melanoma of C57BL/6 mice. In this model 1×10^6 B16.F10 luc$^+$ melanoma cells were injected subcutaneously. Mice received 100 μl intraperitoneal injections of PD-1 blocking antibody or Isotype control on days 1, 4, and 8 and received 100 mg per kg body weight of MDM2-inhibitor RG7112 (n=3) or vehicle (n=2) via oral gavage every second day on day 2–12 (6 doses) following transplantation of melanoma cells.

Tumors were collected on day 13 after melanoma injection. Tile display shows the most significantly differentially regulated genes as determined from robust multichip average (RMA) signal values. The scale represents the level of gene expression with red being highest and blue being lowest. Heatmaps show all significantly regulated genes that belong to IFN-g signaling **(A)** and inflammatory signaling **(B)**. Red arrows point towards genes related to IFN signatures.

(C-F) Fold change bar diagram and representative flow cytometry histogram show the mean fluorescence intensity (MFI) for MHC-II on B16.F10 cells after treatment with DMSO or the indicated concentrations of MDM2-inhibitor HDM201 **(C, D)** or RG7112 **(E, F)** for 72 hours. The experiment was repeated n=10–11 times and the results (mean ± s.e.m.) were pooled. The *p*-values were calculated using a One-way ANOVA and a Dunnett's multiple comparisons or a Kruskal Wallis and a Dunn's multiple comparison test. *ns* = not significant.

(G, H) Fold change diagram and Western blot show the MDM2 and p53 protein levels of a representative experiment with primary human melanoma cell lines treated with DMSO or 0.5 μM RG7112 for 72 hours. Each data point represents an individual patient-derived cell line (n=8). Intensities of protein bands were normalized to Vinculin. The *p*-values were calculated using a one sample *t*-test.

(I) Correlation between the expression of MDM2 and genes making up the IFN-alpha pathway in 469 pre-treatment melanoma patients. R: Pearson's correlation coefficient. The *p*-values are derived from linear models.

(J) Heatmap of genes expressed in the IFN-alpha pathway among "high" and "low" expressors of MDM2. These groups are the top and bottom quartiles of the 469-patient pre-treatment melanoma cohort. Patients are ordered by unsupervised hierarchical clustering.

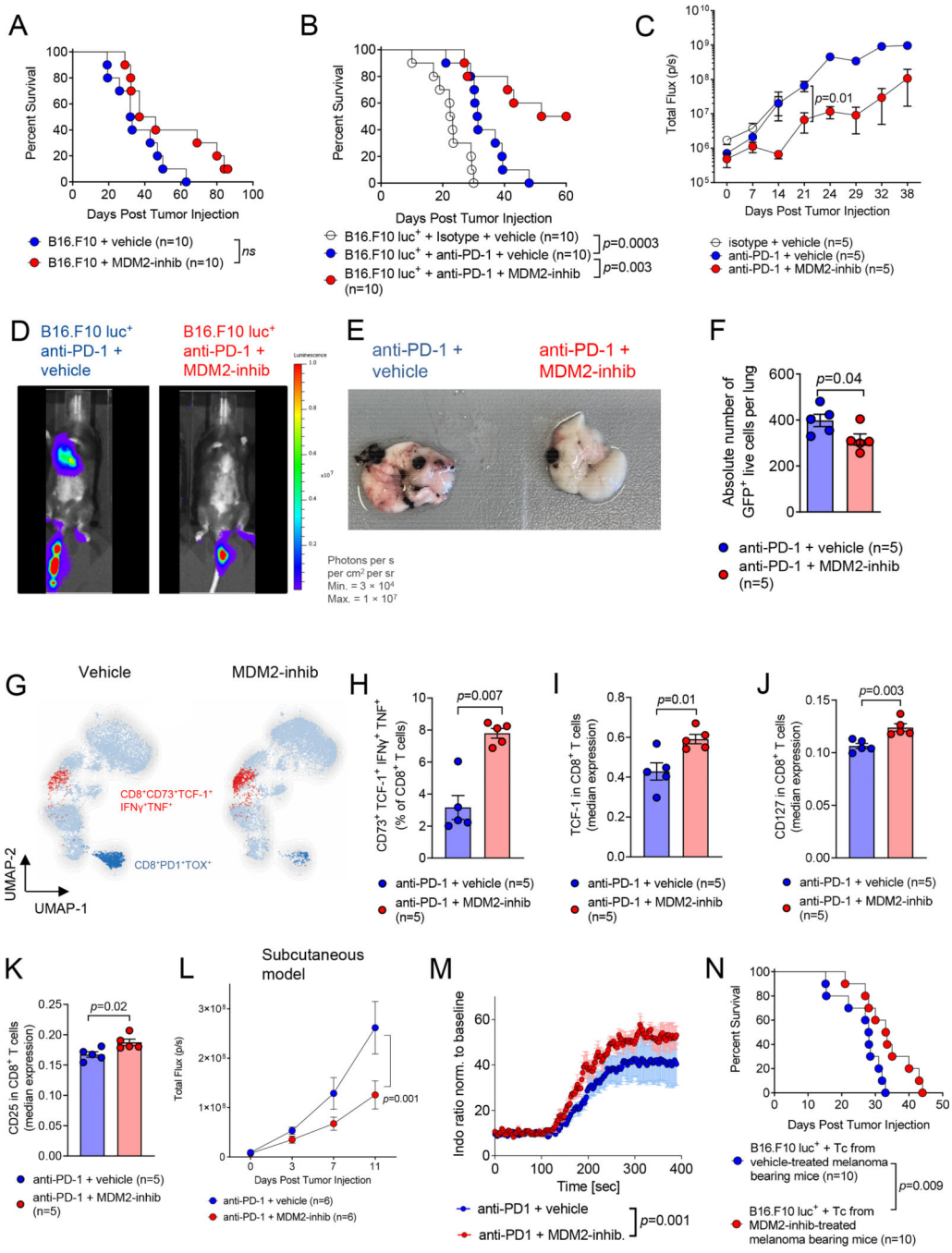

Fig. 2: MDM2-inhibition improves anti-melanoma immune responses in vivo and increases the frequency of CD8$^+$CD73$^+$TCF-1$^+$IFNγ$^+$TNF$^+$ T cells.

(A) Percentage survival of C57BL/6 mice after transfer of 10 000 B16.F10 melanoma cells is shown. Mice received 100 mg per kg body weight of MDM2-inhibitor RG7112 or vehicle via oral gavage every second day on day 2–10 (5 doses) following transplantation of melanoma cells. n=10 animals per group from 2 experiments are shown and *p*-values were calculated using the two-sided Mantel-Cox test. *ns* = not significant.

(B) Percentage survival of C57BL/6 mice after transfer of 5 000 B16.F10 melanoma cells per mouse is shown. Mice received 100 µl intraperitoneal injections of PD-1 blocking

antibody or Isotype control on days 1, 4, 8, 16 and 22 and received 100 mg per kg body weight of MDM2-inhibitor RG7112 or vehicle via oral gavage every second day on day 2–10 (5 doses) following transplantation of melanoma cells. n=10 animals per group from 2 experiments are shown and *p*-values were calculated using the two-sided Mantel-Cox test.

(C) The graph shows the photon flux (p/s/mouse) of C57BL/6 mice after transfer of B16.F10 luc$^+$ melanoma. In this model 10 000 B16.F10 luc$^+$ melanoma cells were injected. Mice received 100 μl intraperitoneal injections of PD-1 blocking antibody or Isotype control on days 1, 4, 8, 16 and 22 and received 100 mg per kg body weight of MDM2-inhibitor RG7112 or vehicle via oral gavage every second day on day 2–10 (5 doses) following transplantation of melanoma cells. For the bioluminescence imaging measurements the following parameters were kept constant for all groups: amount of luciferin injected, type of luciferin, exposure time and distance to camera. The means +/− s.e.m. are shown. n=10 animals per group from 2 experiments are shown and *p*-values were calculated using two-sided Student's unpaired *t*-test.

(D) Representative bioluminescence images of mice described in **(C)** taken 28 days after tumor injection are shown.

(E) Representative images of the lungs of C57BL/6 mice 23 days after transfer of 10 000 B16.F10 melanoma cells. Mice received 100 μl intraperitoneal injections of PD-1 blocking antibody or Isotype control on days 1, 4, 8, 16 and 22 and received 100 mg per kg body weight of MDM2-inhibitor RG7112 or vehicle via oral gavage every second day on day 2–10 (5 doses) following transplantation of melanoma cells.

(F) The scatter bar graph shows the quantification of GFP$^+$ B16 melanoma cells detected in the lungs of C57BL/6 mice 23 days after transfer of 10 000 B16.F10-GFP$^+$ melanoma cells. Mice received 100 μl intraperitoneal injections of PD-1 blocking antibody on days 1, 4, 8, 16 and 22 and received 100 mg per kg body weight of MDM2-inhibitor RG7112 or vehicle via oral gavage every second day on day 2–10 (5 doses) following transplantation of melanoma cells.The means +/− s.e.m. are shown. The *p*-values were calculated using two-sided Student's unpaired *t*-test (n=5 mice per group).

(G) Uniform manifold approximation and projection (UMAP) map displaying randomly sampled cells from the lung CD8$^+$ T cell compartment of B16.F10 melanoma-bearing C57BL/6 mice treated with anti-PD-1 and vehicle or MDM2-inhibitor (RG7112) analyzed by flow cytometry. Colors correspond to FlowSOM-guided clustering of cell populations. In this model 10 000 B16.F10 luc$^+$ melanoma cells were injected. Mice received 100 μl intraperitoneal injections of PD-1 blocking antibody on days 1, 4, and 8 and received 100 mg per kg body weight of MDM2-inhibitor RG7112 or vehicle via oral gavage every second day on day 2–12 (6 doses) following transplantation of melanoma cells. Lungs were collected on day 13 after melanoma injection.

(H) Scatter bar graph displaying the frequency of CD8$^+$CD73$^+$TCF-1$^+$IFNγ^+TNF$^+$ T cells from the metastatic lungs of B16.F10 melanoma-bearing C57BL/6 mice. In this model 10 000 B16.F10 luc$^+$ melanoma cells were injected. Mice received 100 μl intraperitoneal injections of PD-1 blocking antibody on days 1, 4, and 8 and received 100 mg per kg body weight of MDM2-inhibitor RG7112 or vehicle via oral gavage every second day on day 2–12 (6 doses) following transplantation of melanoma cells. Lungs were collected on day 13 after melanoma injection. Cells were stimulated using a Cell Stimulation Cocktail (plus

protein transport inhibitors). Statistical analysis was performed using an unpaired Student's *t*-test (n=5 mice per group, from one experiment).

(I) The scatter bar graph shows the median expression of TCF-1 in $CD8^+$ T cells from the metastatic lungs of B16.F10 melanoma-bearing C57BL/6 mice. In this model 10 000 B16.F10 luc^+ melanoma cells were injected. Mice received 100 µl intraperitoneal injections of PD-1 blocking antibody on days 1, 4, and 8 and received 100 mg per kg body weight of MDM2-inhibitor RG7112 or vehicle via oral gavage every second day on day 2–12 (6 doses) following transplantation of melanoma cells. Lungs were collected on day 13 after melanoma injection. Cells were stimulated using a Cell Stimulation Cocktail (plus protein transport inhibitors). Statistical analysis was performed using an unpaired Student's *t*-test (n=5 mice per group, from one experiment).

(J) The scatter bar graph shows the median expression of CD127 in $CD8^+$ T cells from the metastatic lungs of B16.F10 melanoma-bearing C57BL/6 mice. In this model 10 000 B16.F10 luc^+ melanoma cells were injected. Mice received 100 µl intraperitoneal injections of PD-1 blocking antibody on days 1, 4, and 8 and received 100 mg per kg body weight of MDM2-inhibitor RG7112 or vehicle via oral gavage every second day on day 2–12 (6 doses) following transplantation of melanoma cells. Lungs were collected on day 13 after melanoma injection. Statistical analysis was performed using an unpaired Student's *t*-test (n=5 mice per group, from one experiment).

(K) The scatter bar graph shows the median expression of CD25 in $CD8^+$ T cells from the metastatic lungs of B16.F10 melanoma-bearing C57BL/6 mice. In this model 10 000 B16.F10 luc^+ melanoma cells were injected. Mice received 100 µl intraperitoneal injections of PD-1 blocking antibody on days 1, 4, and 8 and received 100 mg per kg body weight of MDM2-inhibitor RG7112 or vehicle via oral gavage every second day on day 2–12 (6 doses) following transplantation of melanoma cells. Lungs were collected on day 13 after melanoma injection. Statistical analysis was performed using an unpaired Student's *t*-test (n=5 mice per group, from one experiment).

(L) The graph shows the photon flux (p/s/mouse) based on bioluminescence measurements of C57BL/6 mice after subcutaneous injection of 1×10^6 B16.F10-luc^+ melanoma cells. Mice received 100 µl intraperitoneal injections of PD-1 blocking antibody on days 1, 4, and 8 and received 100 mg per kg body weight of MDM2-inhibitor RG7112 or vehicle via oral gavage every second day on day 2–12 (6 doses) following transplantation of melanoma cells. For the bioluminescence imaging measurements the following parameters were kept constant for all groups: amount of luciferin injected, type of luciferin, exposure time and distance to camera. The means +/− s.e.m. are shown. n=6 animals per group are shown and *p*-values were calculated using two-sided Student's unpaired *t*-test.

(M) The graph shows the calcium influx in T cells isolated from B16.F10 melanoma-bearing. In this model 10 000 B16.F10 luc^+ melanoma cells were injected. Mice received 100 µl intraperitoneal injections of PD-1 blocking antibody on days 1, 4, and 8 and received 100 mg per kg body weight of MDM2-inhibitor RG7112 or vehicle via oral gavage every second day on day 2–12 (6 doses) following transplantation of melanoma cells. T cells were isolated from spleens on day 13 after melanoma injection. After one minute of baseline measurement, T cells were stimulated with 3 µg/ml anti-mCD3ε. Pooled data for n=3 mice per group are shown. Statistical analysis was performed using an unpaired Student's *t*-test. Mean values ± s.e.m. are shown.

(N) Percentage survival of C57BL/6 recipient mice after transfer of 10 000 B16.F10 melanoma cells is shown. Mice were sub-lethally irradiated and injected with additional syngeneic T cells (C57BL/6) from spleens harvested on day 12 after melanoma injection (day 2 after melanoma injection of recipient mice). Syngeneic T cells were derived from B16.F10 melanoma-bearing mice that had been treated with MDM2-inhibitor RG7112 or vehicle for 5 times every second day. n=10 animals per group from 2 experiments are shown and *p*-values were calculated using the two-sided Mantel-Cox test.

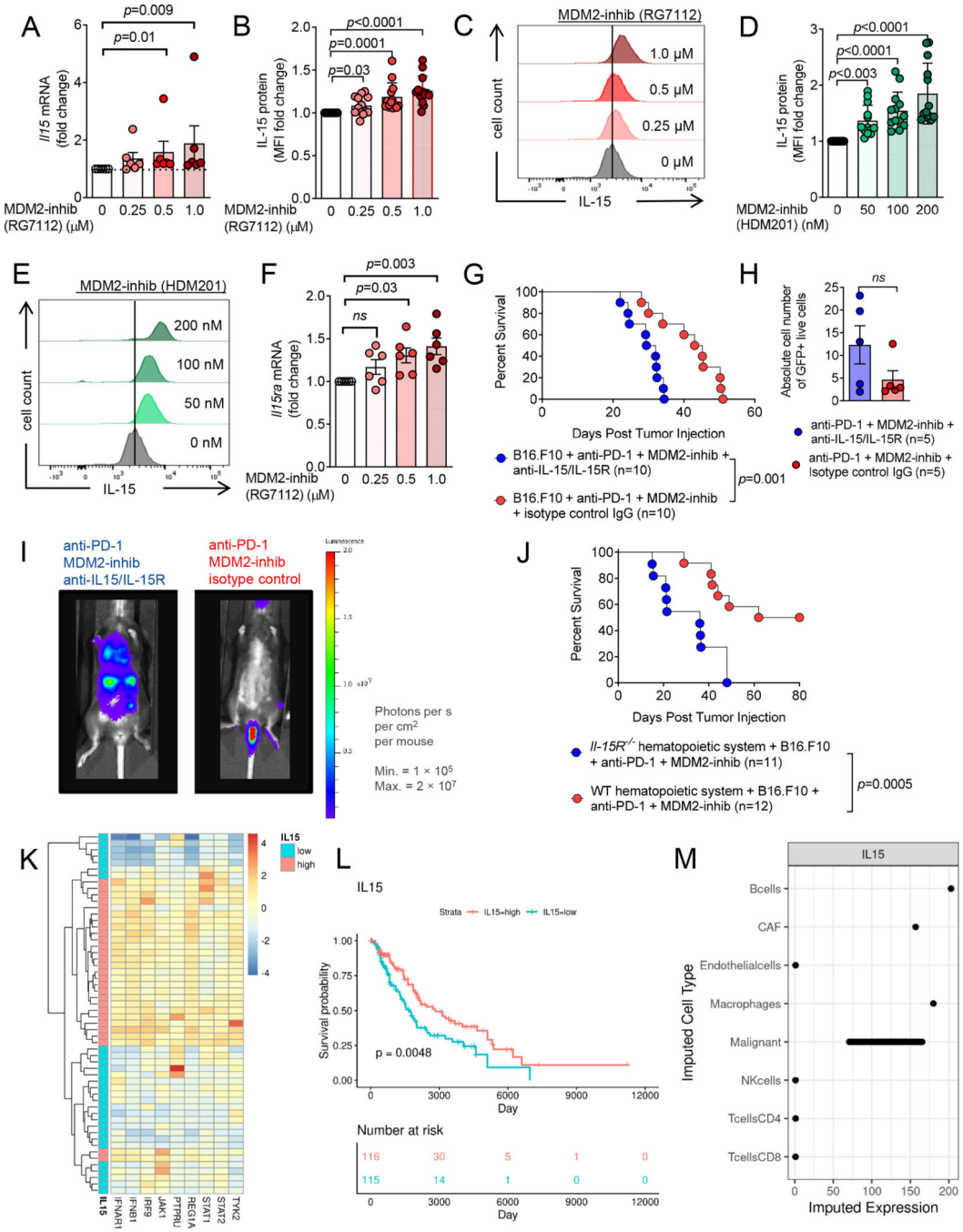

Fig. 3: IL-15 is induced by MDM2-inhibition and hematopoietic IL-15R−/− mice exhibit reduced protective effects of MDM2-inhibition.

(A) The scatter bar graph shows fold changes of Il15 mRNA expression levels in B16.F10 cells, as determined by qPCR, after *in vitro* treatment with MDM2-inhibitor RG7112 at the indicated concentrations for 24 hours. Ct values were normalized to Mon2 and/or Hprt expression as housekeeping genes. Fold changes were calculated relative to DMSO treated control. The experiment was repeated n=6 times and the results (mean ± s.e.m.) were

pooled. Significance was calculated with the Kruskal-Wallis test and individual *p*-values using the Dunn's multiple comparison test. *ns* = not significant.

(B-E) The scatter bar graphs and representative flow cytometry histograms show the mean fluorescence intensity (MFI) for IL-15 in B16.F10 cells after treatment with the indicated concentrations of DMSO or MDM2-inhibitor RG7112 **(B, C)** or HDM201 **(D, E)** for 72 hours. Cells were stimulated using BD Golgi Plug for 5 h. The experiment was repeated n=10–11 times and the results (mean ± s.e.m.) were pooled. The *p*-values were calculated using the Kruskal-Wallis and the Dunn's multiple comparisons test.

(F) The scatter bar graph shows *Il15ra* mRNA expression levels in B16.F10 cells determined by qPCR after *in vitro* treatment with DMSO or the indicated concentrations of MDM2-inhibitor RG7112 for 24 hours. Ct values were normalized to *Mon2* and/or *Hprt* mRNA expression as housekeeping genes. Fold changes were calculated relative to DMSO treated control. The experiment was repeated n=6 times and the results (mean ± s.e.m.) were pooled. Significance was calculated with the one-way ANOVA and individual *p*-values using the Dunnett's multiple comparison test. *ns* = not significant.

(G) Percentage survival of C57BL/6 mice injected with 5 000 B16.F10 melanoma cells. Mice received 100 µl intraperitoneal injections of PD-1 blocking antibody on days 1, 4, 8, 16 and 22 and received 100 mg per kg body weight of MDM2-inhibitor RG7112 via oral gavage every second day on day 2–10 (5 doses) along with 100 µl intraperitoneal injections of nonspecific IgG or anti-IL-15/IL-15R antibody on days 2, 7 and 15 following transplantation of melanoma cells. n=10 independent animals per group from 2 experiments are shown and the *p*-value was calculated using the two-sided Mantel-Cox test.

(H) The scatter bar graph shows the quantification of GFP^+ B16 melanoma cells detected in the lungs of C57BL/6 mice 23 days after transfer of 5 000 B16.F10-GFP^+ melanoma cells. Mice received 100 µl intraperitoneal injections of PD-1 blocking antibody on days 1, 4, 8, 16 and 22 and received 100 mg per kg body weight of MDM2-inhibitor RG7112 via oral gavage every second day on day 2–10 (5 doses) following transplantation of melanoma cells along with 100 µl intraperitoneal injections of nonspecific IgG or anti-IL-15/IL-15R antibody on days 2, 7 and 15 following transplantation of melanoma cells. Lungs were isolated on day 23 after melanoma injection. The means +/− s.e.m. are shown. The *p*-value was calculated using the Mann-Whitney test (n=5 mice per group). *ns* = not significant.

(I) Representative bioluminescence images of C57BL/6 mice injected with 5 000 B16.F10 luc^+ melanoma cells. Mice received 100 µl intraperitoneal injections of PD-1 blocking antibody on days 1, 4, 8, 16 and 22 and received 100 mg per kg body weight of MDM2-inhibitor RG7112 via oral gavage every second day on day 2–10 (5 doses) along with 100 µl intraperitoneal injections of nonspecific IgG or anti-IL-15/IL-15R antibody on days 2, 7 and 15 following transplantation of melanoma cells. For the bioluminescence imaging measurements the following parameters were kept constant for both groups: amount of luciferin injected, type of luciferin, exposure time and distance to camera.

(J) Percentage survival of chimera mice with a hematopoietic system from C57BL/6 *IL-15Ra*$^{-/-}$ or C57BL/6 WT mice as indicated. Survival after transfer of 10 000 B16.F10 melanoma cells is shown. Mice received 100 µl intraperitoneal injections of PD-1 blocking antibody on days 1, 4, 8, 16 and 22 and received 100 mg per kg body weight of MDM2-inhibitor RG7112 via oral gavage every second day on day 2–10 (5 doses) following

transplantation of melanoma cells. n=11–12 animals per group from one experiment are shown and *p*-values were calculated using the two-sided Mantel-Cox test.

(K) Heatmap of genes expressed in the type I Interferon pathway among “high” and “low” expressors of IL-15. These groups are the top and bottom quartiles of the 469-patient pre-treatment melanoma cohort. Patients are ordered by unsupervised hierarchical clustering.

(L) Survivorship differences between “high” and “low” expressors of IL-15. The *p*-value was obtained using the Log-Rank test.

(M) Imputed expression of IL-15 in a set of cell types inferred by deconvoluting bulk RNAseq data.

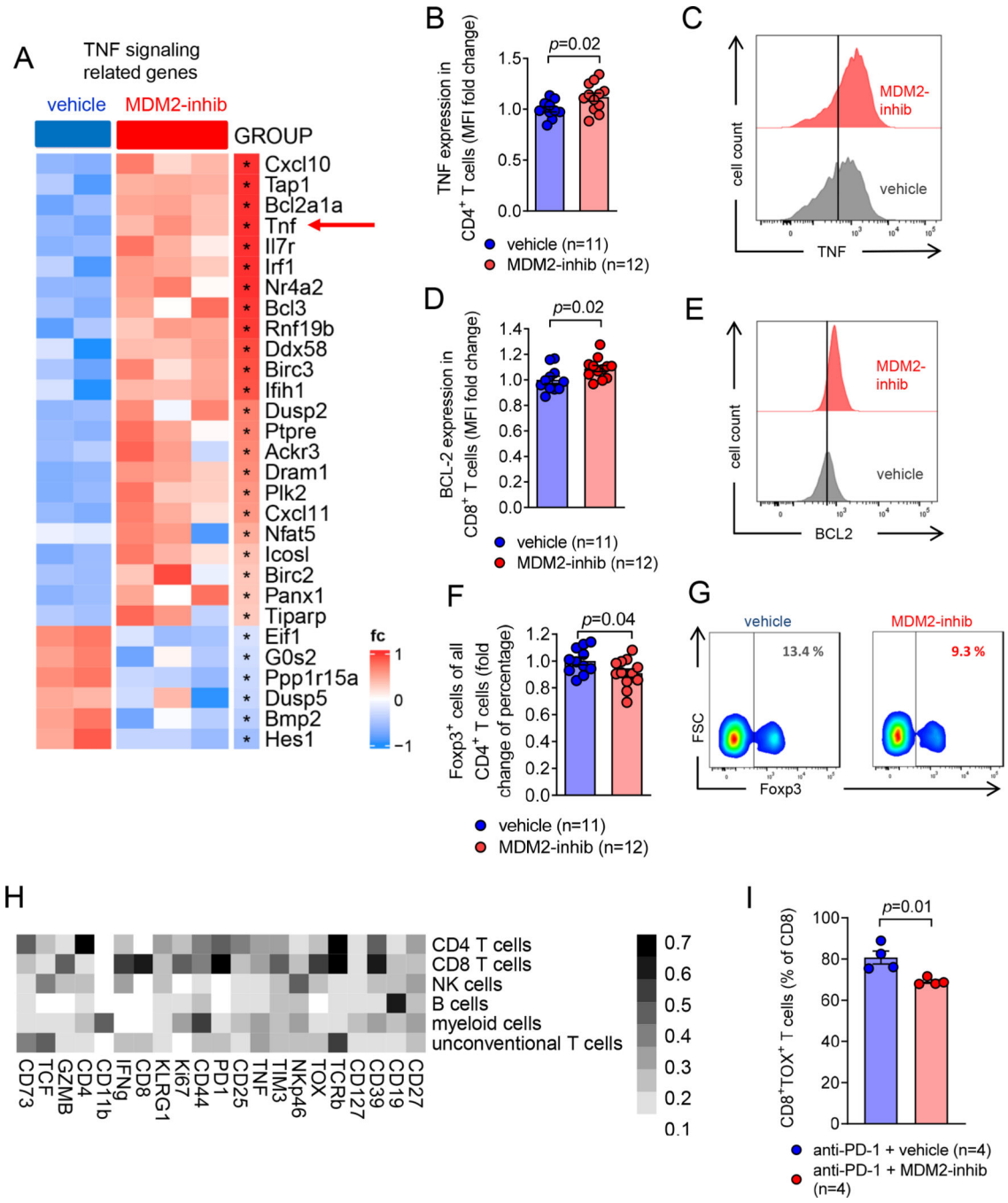

Fig. 4: TNF and TNF-signaling related genes increase upon MDM2-inhibition in the tumor microenvironment while Treg and CD8+TOX+ exhausted T cell frequencies decrease.

(A) Relative expression, as microarray heatmap ("Z-score intensity"), of RNA isolated from subcutaneous B16.F10 melanoma of C57BL/6 mice. In this model 1×10^6 B16.F10 luc$^+$ melanoma cells were injected subcutaneously. Mice received 100 µl intraperitoneal injections of PD-1 blocking antibody on days 1, 4, and 8 and received 100 mg per kg body weight of MDM2-inhibitor RG7112 (n=3) or vehicle (n=2) via oral gavage every second day on day 2–12 (6 doses) following transplantation of melanoma cells. Tumors were collected

on day 13 after melanoma injection. Tile display shows the most significantly differentially regulated genes as determined from robust multichip average (RMA) signal values. The scale represents the level of gene expression with red being highest and blue being lowest. Red arrow points towards the increased expression of Tnf.

(B-G) Scatter bar graphs and representative flow cytometry histograms or frequencies show expression of TNF-α **(B, C)**, BCL-2 **(D, E)** and Foxp3 **(F-G)** of $CD4^+$ or $CD8^+$ T-cells isolated from spleen on day 12 following transfer of 10 000 B16.F10 melanoma cells in C57BL/6 mice. Mice received 100 mg per kg body weight of MDM2-inhibitor RG7112 or vehicle via oral gavage every second day on day 2–10 (5 doses) following transplantation of melanoma cells. Fold change of TNF-α and BCL-2 MFI in $CD4^+$ and $CD8^+$ T-cells, respectively, **(B, D)** or fold change of percentages of $Foxp3^+$ cells of all $CD4^+$ T-cells **(F)** is shown in relation to the mean of vehicle control samples. Cells were stimulated using a Cell Stimulation Cocktail (plus protein transport inhibitors). Mean value ± s.e.m. from n=11–12 animals per group are shown and *p*-values were calculated using two-sided Student's unpaired *t*-test.

H) Heatmap displaying the median marker expression of tumor infiltration $CD45^+$ cells from B16.F10 melanoma injected mice. In this model 1×10^6 B16.F10 luc^+ melanoma cells were injected subcutaneously. Mice received 100 μl intraperitoneal injections of PD-1 blocking antibody on days 1, 4, and 8 and received 100 mg per kg body weight of MDM2-inhibitor RG7112 or vehicle via oral gavage every second day on day 2–12 (6 doses) following transplantation of melanoma cells. Tumors were collected on day 13 after melanoma injection (n=4 mice per group, from one experiment).

(I) Scatter bar graph displaying the frequency of $CD8^+$ TOX^+ T cells isolated from tumors of subcutaneous B16.F10 melanoma injected mice. In this model 1×10^6 B16.F10 luc^+ melanoma cells were injected subcutaneously. Mice received 100 μl intraperitoneal injections of PD-1 blocking antibody on days 1, 4, and 8 and received 100 mg per kg body weight of MDM2-inhibitor RG7112 or vehicle via oral gavage every second day on day 2–12 (6 doses) following transplantation of melanoma cells. Tumors were collected on day 13 after melanoma injection. Cells were stimulated using a Cell Stimulation Cocktail (plus protein transport inhibitors). Statistical analysis was performed using an unpaired Student's *t*-test (n=4 mice per group, from one experiment).

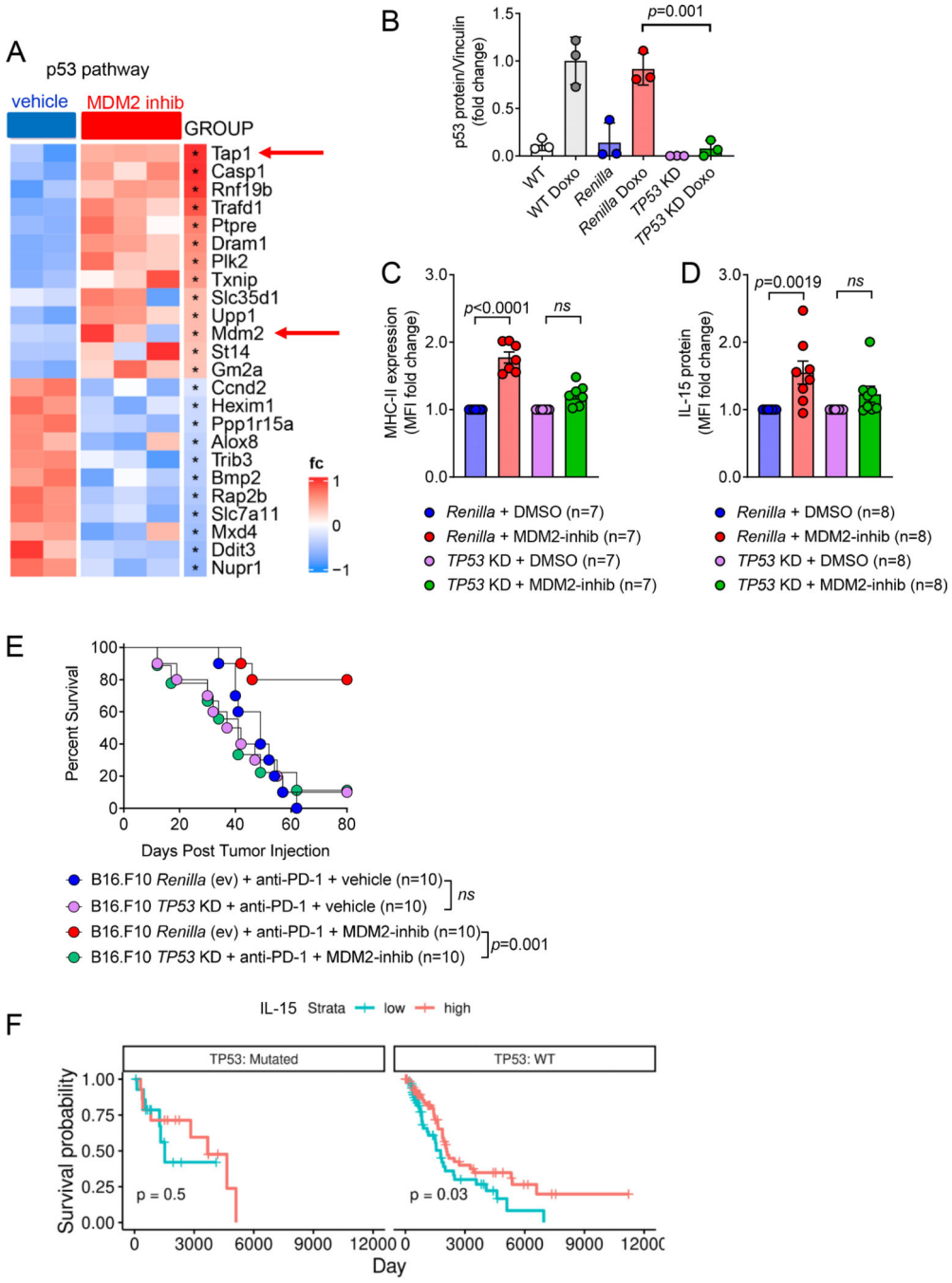

Fig. 5: MDM2-inhibition affects p53 pathway activity in the melanoma micro-environment.

(A) Relative expression, as microarray heatmap ("Z-score intensity"), of RNA isolated from subcutaneous B16.F10 melanoma of C57BL/6 mice. In this model 1×10^6 B16.F10 luc$^+$ melanoma cells were injected subcutaneously. Mice received 100 µl intraperitoneal injections of PD-1 blocking antibody on days 1, 4, and 8 and received 100 mg per kg body weight of MDM2-inhibitor RG7112 (n=3) or vehicle (n=2) via oral gavage every second day on day 2–12 (6 doses) following transplantation of melanoma cells. Tumors were collected on day 13 after melanoma injection. Tile display shows the most significantly differentially

regulated genes as determined from robust multichip average (RMA) signal values. The scale represents the level of gene expression with red being highest and blue being lowest. Red arrows point towards important genes related to the p53 pathway.

(B) The scatter bar graph shows p53 protein intensities relative to Vinculin determined by Western blotting. Cell lysates were prepared after growing wildtype, *Renilla* control shRNA and *TP53* KD B16.F10 with or without 0.5 μM Doxorubicin for 24 hours. The experiment was repeated n=6 times and the results (mean ± s.e.m.) were pooled. The *p*-value was calculated using a two-sided unpaired t-test.

(C, D) MFI of MHC-II **(C)** and IL-15 **(D)** expression are shown on *Renilla* shRNA and *TP53* KD B16.F10 cells after *in vitro* treatment with 1 μM MDM2-inhibitor (RG7112) for 72 hours. Fold changes were calculated relative to DMSO treated controls. Cells for intracellular IL-15 staining were stimulated using BD Golgi Plug for 5 h. The experiment was repeated n=7–8 times and the results (mean ± s.e.m.) were pooled. Significance was calculated using the Kruskal-Wallis test and individual *p*-values using the Dunn's multiple comparison test. *ns* = not significant.

(E) Percentage survival of C57BL/6 mice after transfer of 5 000 murine WT or *TP53* knockdown B16.F10 melanoma cells is shown. Mice received 100 μl intraperitoneal injections of PD-1 blocking antibody on days 1, 4, 8, 16 and 22 and received 100 mg per kg body weight of MDM2-inhibitor RG7112 or vehicle via oral gavage every second day on day 2–10 (5 doses) following transplantation of melanoma cells. n=10 animals per group from 2 experiments are shown and *p*-values were calculated using the two-sided Mantel-Cox test. *ns* = not significant.

(F) Survivorship differences between "high" and "low" expressors of IL-15, as sorted by *TP53* mutation status. Patients were first separated into wild type and mutated cohorts, and then the top and bottom quartile of each cohort was assigned "high" or "low" expressor status. The *p*-values were obtained using the Log-Rank test.

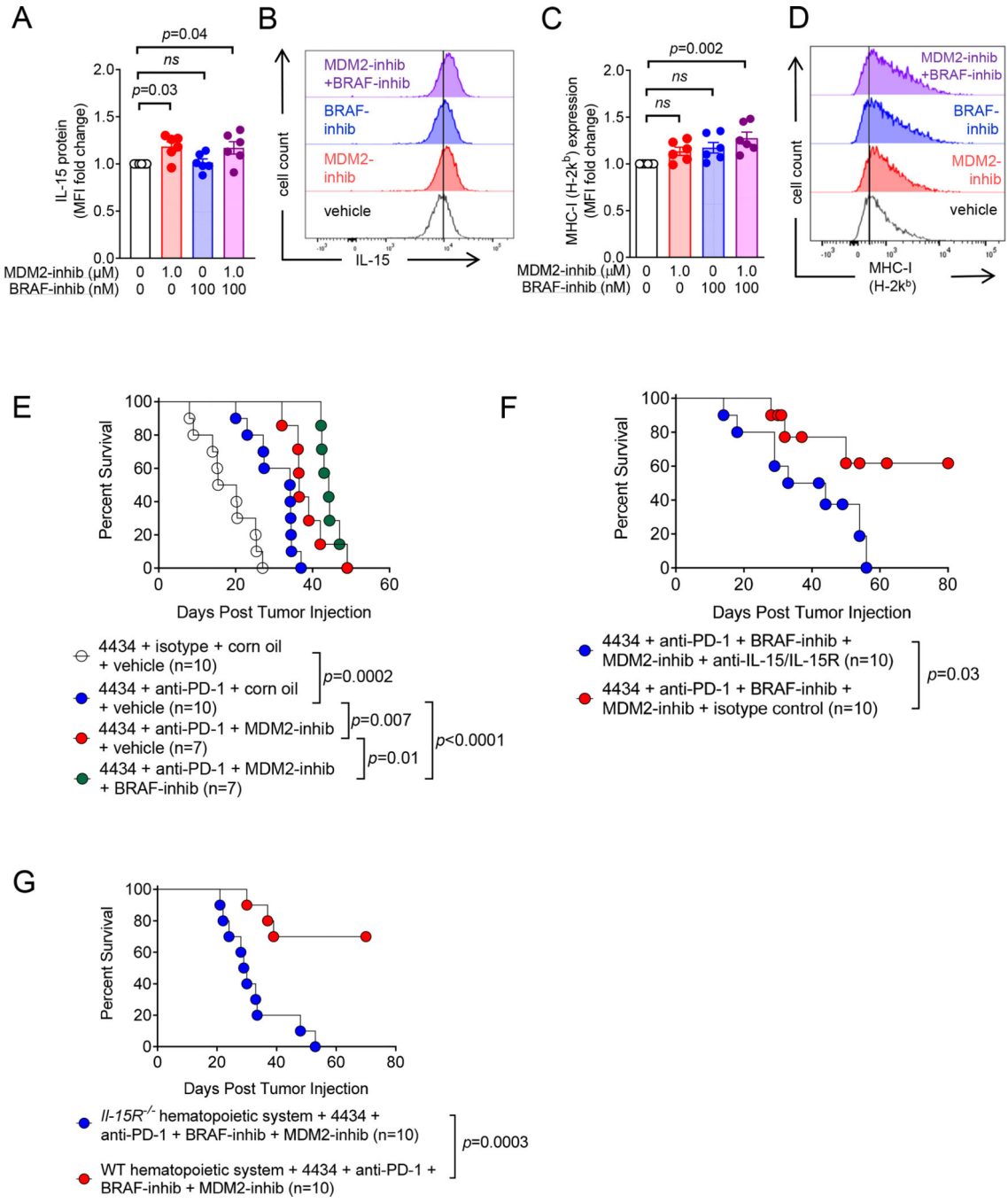

Fig. 6: MDM2-inhibition and BRAF-inhibition act in synergy in *BRAF*^{V600E} mutated melanoma.

(A, C) Scatter bar graphs show the mean fluorescence intensity (MFI) for IL-15 **(A)** and H-2K^b **(C)** on 4434 *BRAF*^{V600E} mutated melanoma cells after treatment with the indicated concentrations of MDM2-inhibitor RG7112 and/or BRAF-inhibitor vemurafenib for 72 hours. Cells for intracellular IL-15 staining were stimulated using BD Golgi Plug for 5 h. The experiment was repeated n=6 times and the results (mean ± s.e.m.) were pooled. Significance was calculated using a one-way ANOVA and individual *p*-values using the Dunnett's multiple comparison test. *ns* = not significant.

(B, D) Flow cytometry histogram shows the mean fluorescence intensity (MFI) for IL-15 **(B)** and H-2K^{b} **(D)** protein on 4434 *BRAF*^{V600E} mutated melanoma cells after treatment with the indicated concentrations of DMSO or MDM2-inhibitor RG7112 for 72 hours of a representative experiment.

(E) Percentage survival of C57BL/6 mice injected with 2×10^{6} 4434 melanoma cells is shown. Mice received 100 μl intraperitoneal injections of PD-1 blocking antibody or Isotype control on days 1, 4, 8, 16 and 22 and received 100 mg per kg body weight of MDM2-inhibitor RG7112 or vehicle via oral gavage every second day on day 2–10 (5 doses) along with 24 mg per kg body weight of BRAF-inhibitor vemurafenib or vehicle via oral gavage every day from day 6–15 (10 doses) following transplantation of melanoma cells. n=7–10 animals per group from 2 experiments are shown and *p*-values were calculated using the two-sided Mantel-Cox test.

(F) Percentage survival of C57BL/6 mice injected with 2×10^{6} 4434 melanoma cells. Mice received 100 μl intraperitoneal injections of PD-1 blocking antibody on days 1, 4, 8, 16 and 22 and received 100 mg per kg body weight of MDM2-inhibitor RG7112 via oral gavage every second day on day 2–10 (5 doses) along with 24 mg per kg body weight of BRAF-inhibitor vemurafenib via oral gavage every day from day 6–15 (10 doses) and 100 μl intraperitoneal injections of nonspecific IgG or anti-IL-15/IL-15R antibody on days 2, 7 and 15 following transplantation of melanoma cells. n=10 independent animals per group from 2 experiments are shown and *p*-values were calculated using the two-sided Mantel-Cox test. Points without vertical drop indicate a censoring event (representing killing of an animal).

(G) Percentage survival of hematopoietic C57BL/6 *IL-15Ra*$^{-/-}$ chimera mice and C57BL/6 WT mice after transfer of 2×10^{6} 4434 melanoma cells (C57BL/6 background) is shown. Mice received 100 μl intraperitoneal injections of PD-1 blocking antibody on days 1, 4, 8, 16 and 22 and received 100 mg per kg body weight of MDM2-inhibitor RG7112 via oral gavage every second day on day 2–10 (5 doses) along with 24 mg per kg body weight of BRAF-inhibitor vemurafenib via oral gavage every day from day 6–15 (10 doses) following transplantation of melanoma cells. n=10 animals per group from 2 experiments are shown and *p*-values were calculated using the two-sided Mantel-Cox test.

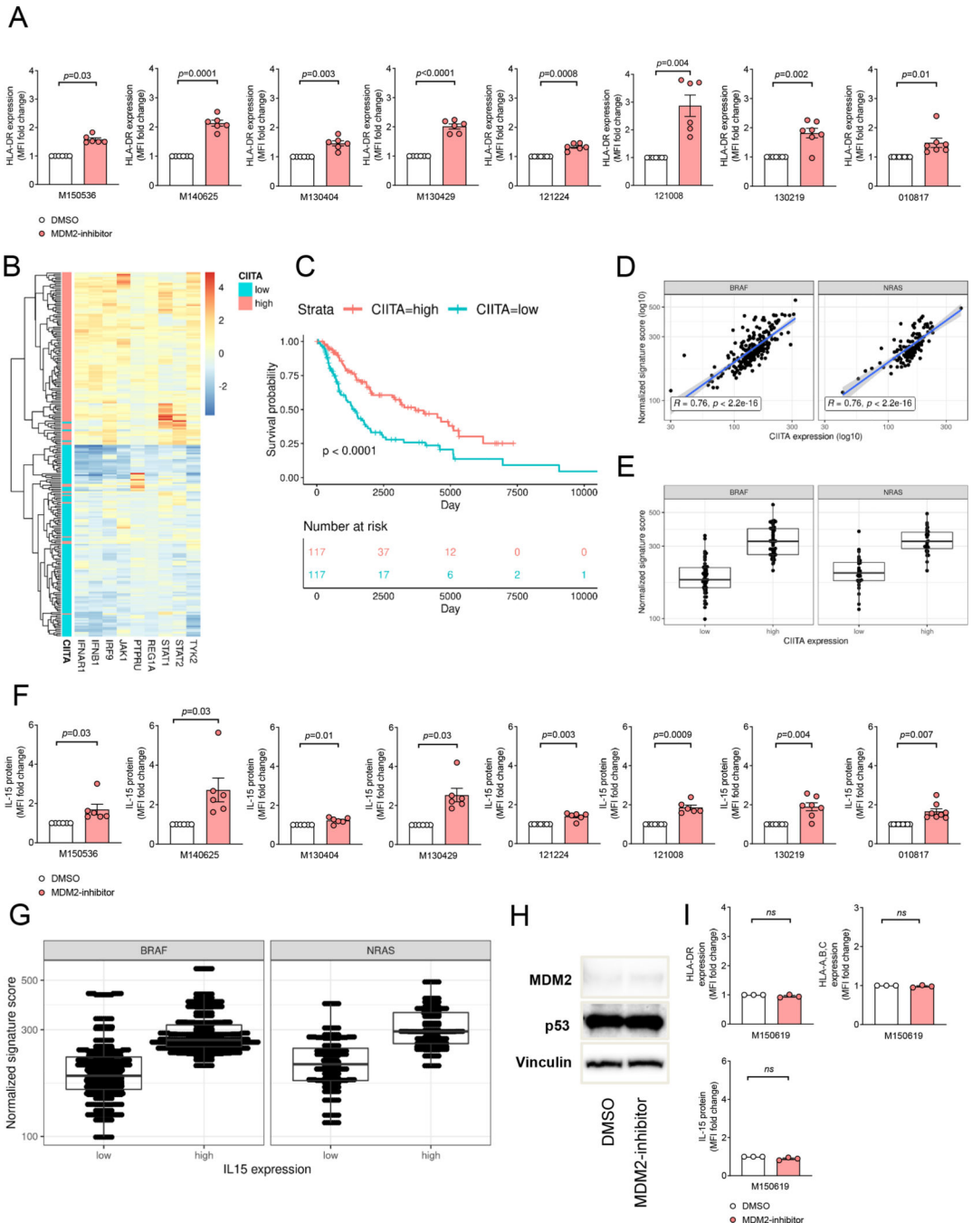

Fig. 7: MDM2-inhibition induces expression of the CIITA / HLA axis in human primary melanoma cells and CIITA-high expression correlates with improved survival in patients.

(A) The scatter bar graphs indicate mean ± s.e.m fold changes of HLA-DR protein levels in 8 human melanoma patient-derived cell lines (M150536, M140625, 121008: *BRAF*^{V600E} mutated, M130404, M130429, 130219, 010817: *NRAS* mutated, 121224: *BRAF*^{V600E} and *NRAS* mutated) assessed by flow cytometry after *in vitro* treatment with MDM2-inhibitor RG7112 at 0.1 – 1 μM for 72 hours (121224, 130227: 0.1 μM, 121008, 130219: 0.25 μM, 010817, M150536, M150619, M140625, M130404, M130429: 0.5 μM, 150672: 1 μM). For individual cell lines non-toxic concentrations of MDM2-inhibitor were employed, as verified

by flow cytometry using viability staining. Fold changes were calculated relative to DMSO treated control. Individual patient-derived cell lines are represented in separate diagrams. The experiments were repeated n=6–7 times and the results (mean ± s.e.m.) were pooled. The *p*-values were calculated using one sample *t*-test or Wilcoxon-test.

(B) Heatmap of genes expressed in the IFN-alpha pathway among “high” and “low” expressors of CIITA. These groups are the top and bottom quartiles of the 469-patient pre-treatment melanoma cohort. Patients are ordered by unsupervised hierarchical clustering.

(C) Survivorship differences between “high” and “low” expressors of CIITA. The *p*-value was obtained using the Log-Rank test.

(D) Correlation between the expression of CIITA and genes making up the IFN-alpha pathway in *BRAF* and *NRAS* mutated melanoma patients. R: Pearson’s correlation coefficient. The *p*-values are derived from linear models.

(E) Normalized IFN-alpha gene set expression scores in *BRAF* and *NRAS* mutated melanoma patients, as compared between the highest and lowest quartiles of expressors of CIITA.

(F) The scatter bar graphs show mean ± s.e.m fold change of IL-15 protein levels in 8 human melanoma patient derived cell lines determined by flow cytometry. Cells were treated *in vitro* with non-toxic concentrations of MDM2-inhibitor RG7112 (0.1 – 0.5 μM) for 72 hours (see **(A)**). Cells were stimulated using BD Golgi Plug for 5 h. Individual patient-derived cell lines are represented in separate diagrams. The experiments were repeated n=6–8 times and the results (mean ± s.e.m.) were pooled. The *p*-values were calculated using one sample *t*-test or Wilcoxon-test.

(G) Normalized IFN-alpha gene set expression scores in *BRAF* and *NRAS* mutated melanoma patients, as compared between the highest and lowest quartiles of expressors of IL-15.

(H) Western blot shows MDM2 and p53 protein expression of a primary human melanoma cell line with a *TP53* mutation after treatment with MDM2-inhibitor RG7112 at 0.5 μM for 72 h.

(I) Scatter bar graphs show mean ± s.e.m fold changes of HLA-A, B, C; HLA-DR and IL-15 protein expression relative to DMSO treated negative control after treatment of a primary human melanoma cell line with *TP53* mutation using the MDM2-inhibitor RG7112. Cells for intracellular IL-15 staining were stimulated using BD Golgi Plug for 5 h. The experiments were repeated n=3 times and the results (mean ± s.e.m.) were pooled. The *p*-values were calculated using a one sample *t*-test. *ns* = not significant.